Controlling ultracold *p*-wave collisions with nonresonant light: Predictions of an asymptotic model

Anne Crubellier,[1,*] Rosario González-Férez,[2,†] Christiane P. Koch,[3,‡] and Eliane Luc-Koenig[1,§]

[1]*Laboratoire Aimé Cotton, CNRS, Université Paris-Sud, Université Paris-Saclay, ENS Paris-Saclay, Faculté des Sciences, Bâtiment 505, 91405 Orsay Cedex, France*

[2]*Instituto Carlos I de Física Teórica y Computacional and Departamento de Física Atómica, Molecular y Nuclear, Universidad de Granada, 18071 Granada, Spain*

[3]*Theoretische Physik, Universität Kassel, Heinrich-Plett-Strasse 40, 34132 Kassel, Germany*

(Received 8 August 2018; revised manuscript received 31 January 2019; published 25 March 2019)

Interactions in a spin-polarized ultracold Fermi gas are governed by *p*-wave collisions and can be characterized by the *p*-wave scattering volume. Control of these collisions by Feshbach resonances is hampered by huge inelastic losses. Here, we suggest nonresonant light control of *p*-wave collisions, exploiting the anisotropic coupling of nonresonant light to the polarizability of the atoms. The *p*-wave scattering volume can be controlled by strong nonresonant light, in close analogy to the *s*-wave scattering length. For collision partners that are tightly trapped, the nonresonant light induces an energy shift directly related to the scattering volume (as defined by A. Crubellier, R. González-Férez, C. P. Koch, and E. Luc-Koenig, preceding paper, Phys. Rev. A **99**, 032709 (2019). This effect could be used to climb the ladder of the trap. We also show that controlling the scattering volume implies control, at least roughly, over the orientation at short interatomic distances of the interparticle axis relative to the polarization direction of the light. Our proposal is based on an asymptotic model that explicitly accounts for the anisotropic dipole-dipole interaction which governs the ultracold collision dynamics at long range.

DOI: 10.1103/PhysRevA.99.032710

I. INTRODUCTION

Collisions of neutral atoms or molecules at very low temperatures are universally described by a single parameter—the *s*-wave scattering length for bosons and unpolarized fermions or the *p*-wave scattering volume for spin-polarized fermions [1]. This parameter is the central quantity of the pseudopotential technique, where the interaction between two particles is accounted for in an effective way through the introduction of contact potentials for each partial ℓ wave [2,3]. The effective interaction in an *s*-wave (resp., *p*-wave) collision vanishes when the scattering length (resp., volume) goes to zero, and likewise it becomes infinite when the scattering parameter becomes infinite. The latter case corresponds to the appearance of a bound state at threshold. The sign of the scattering parameter renders the interaction to be effectively attractive or repulsive, deciding, for example, the stability of a Bose-Einstein condensate or a degenerate Fermi gas against collapse at large densities. Given this prominence, it is not surprising that controlling the scattering length or scattering volume has long been a primary goal in quantum gas experiments.

Initial proposals to control ultracold collisions of neutral atoms focused on near-resonant optical manipulation of the scattering length [4,5]. This type of control is universal since it requires only a suitable optical transition. However, due to inevitable spontaneous emission losses in near-resonant coupling schemes, magnetic field control of Fano-Feshbach resonances has become the most widely employed method of choice to control collisions, in particular for alkali-metal atoms [6]. It requires presence of a hyperfine manifold and sufficiently broad resonances. However, for *p*-wave collisions, enormous inelastic losses were observed near Fano-Feshbach resonances that can only be suppressed in specific geometries [7–12]. Even more severely, species other than the alkali metals, such as alkaline-earth atoms or mixtures of alkali and alkaline-earth atoms, either do not possess Fano-Feshbach resonances at all or their resonances are too narrow to be exploited in magnetic field control. These species are promising candidates for important applications such as optical clocks or quantum simulation. Near-resonant optical control schemes have therefore been revisited [13–15], albeit with mixed success due to spontaneous emission losses.

Spontaneous emission is minimized for nonresonant light control [16,17]. Nonresonant light universally couples to the polarizability of the atoms, independent of the frequency of the light and the energy level structure of the atoms, as long as the frequency remains far detuned from any resonance. This interaction can be used to modify both shape and Fano-Fesbach resonances [16–18]. Moreover, for sufficiently high intensity, the nonresonant light coupling results in a variation of the scattering length with the field intensity [17], similar to the control of the scattering length by a magnetic field near a Fano-Feshbach resonance [6]. This gives rise to nonresonant light control of the scattering length [19]. In particular, the scattering length diverges when, with increasing intensity, a shape resonance crosses the threshold to become bound or when the field-dressed potential becomes sufficiently deep-

*anne.crubellier@u-psud.fr
†rogonzal@ugr.es
‡christiane.koch@uni-kassel.de
§eliane.luc@u-psud.fr

ened to accommodate an additional bound level [16,18]. It is natural to ask whether this type of control can be extended to p-wave collisions of spin-polarized fermions.

To answer this question, we employ an asymptotic model which replaces the interaction potential by its asymptotic part [20–25]. This approximation is well justified at ultralow temperatures. When controlling a pair of atoms with nonresonant light, the resulting asymptotic Hamiltonian [18,19] turns out to be identical to the one describing the control of atom-atom interaction by a static electric field [26] as well as that describing ultracold collisions of polar molecules [27,28]. These problems have in common that they are all governed by the anisotropic dipole-dipole interaction, which decreases with the interatomic separation as $1/R^3$ and introduces a coupling between all partial ℓ waves of the same parity. The crucial parameter of the corresponding asymptotic model is the p-wave scattering volume which may, on first glance, appear to be ill defined in the presence of dipole-dipole interaction. However, we have shown in the preceding paper of this issue, referred to as Paper I [29], how to remedy this problem by suitably generalizing the definition of the scattering volume. We can thus proceed now to examine nonresonant light control of the scattering volume that involves exactly this type of interaction.

The present paper is organized as follows. Section II recalls the asymptotic model for an interparticle interaction of dipole-dipole type in Sec. II A and lists a few typical physical examples of this model in Sec. II B. We use the asymptotic model to make general predictions for nonresonant light control of the scattering volume in Sec. III, distinguishing between weak and strong confinement in Secs. III A and III B. Section IV analyzes the connection between controlling the scattering volume and the orientation of the interparticle axis relative to the polarization direction for the pure p-wave case in Sec. IV A and for multiple channels in Sec. IV B. We conclude in Sec. V.

II. MODEL

A. Hamiltonian and asymptotic Schrödinger equation

The model describing the relative motion of two dipoles aligned along the laboratory Z axis and interacting via a short-range potential is close to the one described in a previous study [19]. For completeness, we briefly recall here the Hamiltonian and the reduced units that allow for a general treatment, independent of the specific parameters of the particles. In the Born-Oppenheimer approximation and employing spherical coordinates, the Hamiltonian reads

$$H = T_R + \frac{\hbar^2 \mathbf{L}^2}{2\mu R^2} + V_g(R) + \mathcal{D}\frac{3\cos^2\theta - 1}{R^3}, \tag{1}$$

where R denotes the interparticle separation and θ is the angle between $\vec{R}$ and the Z axis. μ is the reduced mass, T_R is the radial kinetic energy, $\mathbf{L}$ is the orbital angular momentum operator, and $V_g(R)$ is the potential describing the short-range interactions. For simplicity, $V_g(R)$ is limited here to the van der Waals potential, $V_g(R) = -C_6/R^6$, with C_6 the van der Waals coefficient. The last term in the Hamiltonian Eq. (1) stands for the anisotropic dipole-dipole interaction governing the scattering properties at large interparticle distance. This interaction can be due to nonresonant light with intensity I which is linearly polarized along the Z axis and couples to the polarizability anisotropy of the particles. Equivalently, it can represent the interactions between particles with permanent electric or magnetic dipole moments aligned by an external electric or magnetic field along the Z axis. The equivalence is expressed in terms of the dipolar interaction strength $\mathcal{D}$,

$$\mathcal{D} \leftrightarrow \frac{1}{4\pi\epsilon_0} d_1 d_2 \leftrightarrow \frac{\mu_0}{4\pi} m_1 m_2 \leftrightarrow \frac{4\pi I}{c}\alpha_1\alpha_2, \tag{2}$$

where $d_{1,2}$ ($m_{1,2}$) denotes the magnitude of the electric (magnetic) dipole moments, whereas $\alpha_{1,2}$ are the static polarizabilities of the two particles, with a dimension of volume [18]. Here, c denotes the velocity of light, ϵ_0 is the permittivity of vacuum, and μ_0 is the vacuum permeability. Assuming electric dipole moments $d_{1,2} = 1\,\mathrm{D}$ or magnetic dipole moments $m_{1,2} = 1\,\mu_B$ with μ_B being the Bohr magneton, the dipolar interaction strength amounts to $241 a_0^5\,\mathrm{s}^{-2}\,\mathrm{kg}$ and $0.0207 a_0^5\,\mathrm{s}^{-2}\,\mathrm{kg}$, respectively. For particles with polarizability $\alpha_{1,2} = 100 a_0^3$ with a_0 being the Bohr radius, submitted to light with intensity $I = 100\,\mathrm{MW/cm^2}$, $\mathcal{D}$ becomes $0.0222 a_0^5\,\mathrm{s}^{-2}\,\mathrm{kg}$. For typical systems, the electric dipolar interaction is thus generally much larger than the magnetic one, and a very high light intensity is required to obtain, for nonresonant light, a dipolar coupling strength similar to that of the magnetic dipole interaction.

The Hamiltonian Eq. (1) commutes with parity and with L_Z, the projection of the orbital angular momentum on the laboratory Z axis. As a result, the projection quantum number m is conserved. Nonresonant light control of the scattering length concerning $m = 0$ and even-parity ℓ states has been discussed in Ref. [19]. Here, we consider odd-parity wave functions with $m = 0$ or ± 1.

A universal form of the Hamiltonian Eq. (1) is obtained by introducing reduced units. These can be chosen to eliminate the scaling factor of the rotational kinetic energy together with the prefactor of either the dipole-dipole interaction or the van der Waals term. In the latter case, hereafter referred to as "van der Waals reduced units" (and denoted by r.u.), the reduced units of length x, energy $\mathcal{E}$, and nonresonant field intensity $\mathcal{I}$ are, respectively, defined by $R = \sigma x$, $E - E_0 = \epsilon\,\mathcal{E}$, where E_0 denotes the shift of the dissociation limit induced by the nonresonant light, and $I = \beta\,\mathcal{I}$ [18,25]. The corresponding characteristic length σ, energy ϵ, and field intensity β are equal to

$$\sigma = \left(\frac{2\mu C_6}{\hbar^2}\right)^{1/4}, \tag{3a}$$

$$\epsilon = \frac{\hbar^2}{2\mu\sigma^2}, \tag{3b}$$

$$\beta = \frac{c}{12\pi}\frac{\hbar^{3/2} C_6^{1/4}}{\alpha_1\alpha_2(2\mu)^{3/4}} = \frac{c\sigma^3\epsilon}{12\pi\alpha_1\alpha_2}. \tag{3c}$$

These unit conversion factors contain all the information specific to the particle species, i.e., reduced mass μ, van der Waals coefficient C_6, and polarizabilities α_1 and α_2. With these units, the asymptotic Schrödinger equation for the wave function $f(x, \theta, \phi)$, where ϕ denotes the azimuthal angle,

TABLE I. Examples of atom pairs which are good candidates for collision control by nonresonant light together with their van der Waals constant C_6, atomic polarizabilities $\alpha_{1,2}$, taken from Ref. [30], and values for the reduced units of length σ, energy ϵ, and intensity β; cf. Eq. (3). The proportionality coefficients that relate the interaction with nonresonant light of intensity $\mathcal{I}$ to the dipole-dipole interaction of a pair with permanent magnetic m or electric d dipole moment [cf. Eq. (2)] are also given.

Pair	C_6 (units of a_0^6)	α_1, α_2 (units of a_0^3)	σ (units of a_0)	ϵ/k_B (μK)	β (GW cm^{-2})	$m/\sqrt{\mathcal{I}}$ (μ_B)	$d/\sqrt{\mathcal{I}}$ (Debye)
$^{88}Sr_2$	3248.97	186.25	151.053	86.365	0.6358	4.858	0.04506
^{86}Sr–^{88}Sr	3248.97	186.25	150.618	87.875	0.6413	4.879	0.04525
$^{86}Sr_2$	3248.97	186.25	150.188	89.393	0.6468	4.900	0.04545
$^{87}Sr_2$	3248.97	186.25	150.623	87.855	0.6412	4.879	0.04525
$^{171}Yb_2$	1932.0	142.0	156.639	41.303	0.5833	3.548	0.03290
$^{172}Yb_2$	1932.0	142.0	158.868	40.943	0.5807	3.540	0.03283
$^{173}Yb_2$	1932.0	142.0	157.096	40.588	0.5782	3.532	0.03276
$^{174}Yb_2$	1932.0	142.0	157.323	40.238	0.5757	3.525	0.03269
^{40}K–^{87}Rb	4106.5	292.88 309.88	142.284	156.282	0.3674	5.975	0.05541
^{7}Li–^{133}Cs	2933.8	163.98 402.20	91.885	1539.41	1.3416	9.731	0.09025
^{87}Rb–^{133}Cs	5284.9	309.98 402.20	178.379	51.802	0.1747	4.828	0.04478
$^{52}Cr_2$	733.0	78.0	91.2731	400.338	3.7071	4.913	0.04556
$^{53}Cr_2$	733.0	78.0	91.7093	389.047	3.6545	4.878	0.04524

becomes

$$\left[-\frac{d^2}{dx^2} - \frac{1}{x^6} + \frac{\mathbf{L}^2}{x^2} - \mathcal{I}\frac{\cos^2\theta - 1/3}{x^3} - \mathcal{E}\right] f(x,\theta,\phi) = 0, \tag{4}$$

where the van der Waals interaction is indeed described by the universal term $-1/x^6$. The nonresonant field intensity $\mathcal{I}$ is a tunable parameter allowing to control the collision. For a dipole-dipole interaction characterized by the strength $\mathcal{D}$, the reduced intensity is $\mathcal{I} = 3\mathcal{D}/\epsilon\sigma^3$.

A second set of reduced units, hereafter referred to as "dipole-dipole units" [and denoted by r.u.(dd)] is better adapted to the analysis of the aligned dipole-dipole interaction [see Eq. (2)]. It is obtained by introducing the characteristic length D and energy E_D [28],

$$D = \frac{\mu}{\hbar^2}\mathcal{D}, \tag{5a}$$

$$E_D = \frac{\hbar^2}{\mu D^2} = \frac{\mathcal{D}}{D^3}, \tag{5b}$$

such that $R = D\bar{x}$ and $E = E_D\bar{\mathcal{E}}$. In these reduced units, the asymptotic Schrödinger equation reads

$$\left[-\frac{d^2}{d\bar{x}^2} - \frac{\bar{c}_6}{\bar{x}^6} + \frac{L^2}{\bar{x}^2} - 6\frac{\cos^2\theta - 1/3}{\bar{x}^3} - 2\bar{\mathcal{E}}\right] f(\bar{x},\theta,\varphi) = 0, \tag{6}$$

where $\bar{c}_6$, the reduced strength of the van der Waals interaction, is given by

$$\bar{c}_6 = 2\mu C_6/(\hbar^2 D^4). \tag{7}$$

Whereas in Eq. (4), the short-range van der Waals interaction is described by a universal term, it is the long-range dipole-dipole interaction which appears as universal in Eq. (6). Converting the characteristic length and energy from one unit set to the other depends only on $\mathcal{I}$,

$$D = \frac{\mathcal{I}}{6}\sigma, \tag{8a}$$

$$E_D = \frac{72}{\mathcal{I}^2}\epsilon, \tag{8b}$$

whereas the nonuniversal system-dependent parameters $\bar{c}_6$ and $\mathcal{I}$ in Eqs. (6) are related by

$$\bar{c}_6 = \frac{\sigma^4}{D^4} = \frac{6^4}{\mathcal{I}^4}. \tag{9}$$

B. Physical examples described by the asymptotic model

We summarize here the physical characteristics and scaling factors for a few atoms and molecules to which our model applies, either when they interact with a nonresonant field, cf. Table I, or with each other via a permanent electric or magnetic dipole moment, that we assume to be completely oriented by an external electric or magnetic field, cf. Table II. Tables I and II present the asymptotic physical properties for the two types of interactions in the corresponding systems of reduced units. This information needs to be complemented by the characteristics of the short-range interactions for a given species, such as the s-wave scattering length. The latter is typically rather difficult to obtain, in both theory and experiment. Here, in order to remain general, we characterize the short-range part by the nodal parameter introduced in Paper I [29], leaving it free to vary such that any actual setting will be covered.

Table I presents our selection of good candidates for control with nonresonant light out of the species that have already experimentally been cooled down to temperatures in the millikelvin or even nanokelvin range. While all atomic or molecular collision partners are polarizable and thus interact with nonresonant light, the field strengths required for control are rather different. For the nonresonant light to significantly

TABLE II. Examples of pairs of molecules and atoms with notable dipole moment, either magnetic m or electric d, and with polarizability α taken from Ref. [30]. The reduced units of length D and energy E_D are specific to the dipole-dipole interaction; see Eq. (5). The value of the van der Waals constant is C_6 given in atomic units and $\bar{c}_6$ in dipole-dipole reduced units [r.u.(dd)]; see Eq. (7). A nonresonant field of intensity $\mathcal{I}_c$ in reduced units (r.u.) specific to the van der Waals interaction, with conversion factor β [see Eq. (3c)] would mimic the effect of the permanent dipole moments; cf. Eq. (10).

Pair	C_6 (units of a_0^6)	m (μ_B)	d (Debye)	α (units of a_0^3)	D (units of a_0)	E_D/k_B (μK)	$\bar{c}_6$ [r.u.(dd)]	$\mathcal{I}_c$ (r.u.)	β (GW cm^{-2})
$(^{40}K–^{87}Rb)_2$	15972.0		0.566	602.86	5734.14	83.0502×10^{-3}	3.41677×10^{-6}	139.556	0.06862
$(^{39}K–^{87}Rb)_2$	15972.0		0.566	602.86	5688.93	85.0461×10^{-3}	3.49889×10^{-6}	138.73	0.06903
$(^{7}Li–^{133}Cs)_2$	4585400		5.5	566.18	597139.	6.944×10^{-6}	9.19856×10^{-12}	3445.25	0.29758
$(^{87}Rb–^{133}Cs)_2$	147260.0		1.23	712.17	46917.3	716.021×10^{-6}	1.21779×10^{-8}	571.161	0.05674
$^{52}Cr_2$	733.0	6.00696		78.0	22.7413	12897.6	259.46	1.4944	3.7071
$^{53}Cr_2$	733.0	6.00696		78.0	22.1792	12180.4	245.05	1.5165	3.6545
$^{161}Dy_2$	1890.0	10.0046		165.0	195.267	56.4625	0.381358	7.63516	0.44952
$^{162}Dy_2$	1890.0	10.0046		165.0	196.663	55.3203	0.372951	7.67783	0.44744
$^{164}Dy_2$	1890.0	10.0046		165.0	199.095	53.3178	0.35945	7.74893	0.44334
$^{167}Er_2$	1760.0	7.00732		153.0	99.3172	210.4070	5.5045	3.9172	0.49965
$^{168}Er_2$	1760.0	7.00732		153.0	99.9123	206.6690	5.4067	3.9348	0.49742
$(^{168}Er_2)^2$	7040.0	14.0046		306.0	799.2990	1.61460	0.0105599	18.718	0.10457

alter the scattering properties, the field-induced term in the Hamiltonian Eq. (1) needs to compete with the rotational kinetic energy. In other words, large polarizabilities and reduced masses are favorable, explaining our choice of strontium [31,32] and ytterbium [33–35]. For even isotopes, these atoms have a closed-shell ground state $^1S_0$ with vanishing total angular momentum $J = 0$ and possess neither a permanent magnetic dipole moment nor a hyperfine manifold. In addition to the atomic homonuclear pairs with no permanent electric or magnetic dipole moment, we consider heteronuclear dialkali-metal pairs with permanent electric dipole moment: the smallest (KRb [36,37]), the largest (LiCs [38]), and an intermediate example (RbCs [39]). Finally, we include the pair of transition-metal atom Cr with atomic ground level $3d^5 4s\,^7S_3$, with a large permanent magnetic dipole moment. For these pairs, the reduced length σ characterizing the range of interatomic separation where the van der Waals interaction prevails is of the order of 100 to 200 a_0. The reduced energy ϵ is in the microkelvin range. The reduced unit of nonresonant light intensity, β, of the order of 1 GW/cm^2, provides an estimate for the intensity required to effectively control the collisions. While such a high intensity is challenging to realize experimentally, a tight focus is one way to reach it, as discussed in Refs. [17,19] for the control of the s-wave scattering length. Application of a nonresonant light of reduced intensity $\mathcal{I}$ is identical to dipole-dipole interaction in systems with a permanent electric d or magnetic m dipole moment, increasing as $\sqrt{\mathcal{I}}$ and proportional to $C_6^{1/8}/(\alpha\mu^{3/8})$; see Eq. (2). For an intensity of $\mathcal{I} = 1$ r.u., i.e., $I = \beta$ GW/cm^2 [with β evaluated from Eq. (3c)], the equivalent electric dipole moments reported in Table I are about 0.03 to 0.1 D, whereas the equivalent magnetic dipole moments are in the range from 3.5 to 10 μ_B. The pair RbCs (Cr_2) presents the largest (smallest) value for the product of the polarizabilities $\alpha_1\alpha_2$ or, equivalently, the smallest (largest) reduced unit for the field intensity β. It is thus the most (least) favorable candidate for control by nonresonant light. Note that the very large values of the equivalent dipole moments for LiCs result from the very small reduced mass μ.

Table II presents the reduced units of length D and energy E_D, cf. Eqs. (5), for collision partners with a permanent electric or magnetic dipole moment, assumed to be aligned. It starts with pairs of heteronuclear dialkali-metal molecules, namely pairs of KRb, LiCs, and RbCs [40,41], in their lowest rovibrational level. These molecules possess a large permanent electric dipole moment varying from $d = 0.56$ D for KRb up to 5.5 D for LiCs (see Table I of Ref. [42]). The polarizability of the diatomic molecule is taken to be equal to the sum of the polarizabilities of the two constituent atoms. For these pairs, the van der Waals interaction in the lowest rovibrational level is huge, three orders of magnitude larger than in a pair of alkali atoms (see Table II of Ref. [42]). However, the reduced strength of the van der Waals interaction $\bar{c}_6$ decreases as $\mu C_6 D^{-4}$; see Eq. (7). Since the unit of length $D \propto \mu d^2$ is also very large, especially for LiCs ($D \sim 0.32\,\mu$m due to large d) and for RbCs ($D \sim 0.25\,\mu$m due to large d and μ), $\bar{c}_6$ takes values between 10^{-11} to 10^{-6} r.u. (dd). Therefore, the van der Waals interaction is almost negligible, and the dipole-dipole interaction governs the dynamics.

Table II also presents homonuclear pairs of atoms, bosonic or fermionic, with a large total angular momentum J and therefore a large permanent magnetic moment: pairs of the transition-metal atom Cr, with atomic ground level $3d^5 4s\,^7S_3$ [43,44], and pairs of the lanthanide atoms Dy [45,46] and Er [47,48], with respective atomic ground levels $4f^{10}6s^2\,^5I_8$ and $4f^{12}6s^2\,^6H_6$. In their lowest state, $^{2S+1}L_J\,|M_J| = J$, with Landé factor g_J, these atoms possess a large permanent magnetic dipole moment $m = \mu_B g_J J$, and two collision partners strongly interact via magnetic dipole-dipole interaction. The van der Waals coefficients for Er and Dy are taken from Refs. [49] and [50], respectively. Finally, Table II considers the collision between two Er_2 molecules [48] oriented by an external magnetic field. The total permanent magnetic dipole moment of the molecule is taken to be equal to twice that of a single atom. The van der Waals coefficient for the collision between two Er_2 molecules is taken equal to four times the van der Waals coefficient between two Er atoms in their ground level.

For the examples with the strongest permanent dipole moments d in Table II, the characteristic distance D is huge and the energy E_D is very small. For instance, the temperature associated to E_D varies from the nanokelvin range for KRb down to the femtokelvin range for LiCs. Simultaneously, the spatial range increases from a few micrometers up to a few millimeters. For magnetic atoms interacting via dipole-dipole interaction, the interaction length is smaller, a few hundred nanometers, corresponding to much higher temperatures, from $\sim 0.1\,\mu$K for Dy up to ~ 0.1 mK for Cr, whereas for molecular partners such as Er_2 it corresponds to microkelvin.

For permanent dipoles, we introduce the critical laser intensity $\mathcal{I}_c$ for which the strength of the nonresonant light interaction becomes equal to the strength of the dipole-dipole interaction. It is important to note that in reduced units the value of the critical intensity does not depend on the polarizabilities,

$$\mathcal{I}_c = \frac{3\,(2\mu)^{3/4}}{\hbar^{3/2} C_6^{1/4}} \mathcal{D}. \tag{10}$$

For collisions between aligned polar molecules, the critical intensity $\mathcal{I}_c$ is rather large, equal to 140, 570, and 3440 r.u. for KRb, RbCs, and LiCs respectively; see Table II. In contrast, for collisions of magnetic atoms, the critical intensity is much smaller, equal to 1.5, 3.9, and 7.7 r.u. for Cr, Er, and Dy atoms. Magnetic molecules represent an intermediate case, with $\mathcal{I}_c = 19$ r.u. for collisions between Er_2 molecules. These differences in $\mathcal{I}_c$ reflect the fact that the strength of the magnetic dipole-dipole interaction between highly magnetic atoms, transition metals and lanthanides, is smaller than the strength of the electric dipole-dipole interaction between molecules with large permanent electric dipole moment.

With a number of good candidates at hand, we proceed to analyze nonresonant light control of the scattering volume. To this end, we need to account for how the particles are trapped.

III. CONTROL OF *p*-WAVE COLLISIONS

When atoms or molecules are confined in a magneto-optical trap (MOT) with an extension of up to a few millimeters, the confinement is very weak and the interparticle distance can be considered to extend to infinity. It is then possible to approximately assume the collision partners to freely move in space. In this case, the asymptotic model with universal nodal lines is used to determine the intensity dependence of a quantity which captures the contributions of the short-range interactions in the case of an asymptotic interaction decreasing as $1/R^3$, that we have defined in Paper I [29] and that we simply call scattering volume in the following.

This quantity is determined (see Paper I [29] for more details) by expanding $f(x, \theta, \phi)$ in Eq. (4) into spherical harmonics $Y_{\ell m}(\theta, \phi)$. A complete set of solutions of the resulting coupled radial equations for a fixed m value is obtained at threshold ($\mathcal{E} = 0$) by inward integration as follows. We start by calculating particular solutions, for which the asymptotic behavior is accounted for in terms of the initial conditions for the integration, with a nonvanishing component only in a particular channel ℓ, with either diverging or nondiverging asymptotic behavior. These particular solutions do not satisfy short-range boundary conditions and their number is twice the number of physical solutions. For the latter, the short-range boundary conditions are given by a vanishing of the solutions on what we call the nodal lines. These consist in energy-, ℓ-, and intensity-dependent positions, characterized by a single parameter that we call the nodal parameter. It captures the influence of the short-range part of the molecular potential that is not considered explicitly in the asymptotic model [51]. We then isolate the physical solution which does not diverge in the channel $\ell = 1$ only. The coefficient of the nondivergent $\ell = 1$ part of this solution depends on $x_{\max}$, the starting point of the integration, in a way which can be approximately predicted by an analytical single channel model, as described in Paper I [29]. Performing several calculations with different $x_{\max}$ allows us to deduce the scattering volume in Paper I [29].

We present results obtained with this procedure in Sec. III A, where we pay particular attention to identifying intensities for which the scattering volume diverges. This corresponds to the presence of a bound state at the dissociation limit and of a shape resonance just above threshold. In contrast, for strong confinement, as realized in an optical dipole trap or in optical lattices, it is no longer possible to consider cold collisions in free space. We examine, in Sec. III B, the case where the characteristic length of the trap (assumed to be isotropic and harmonic) is larger than σ, limiting the nonresonant field intensity to relatively small values, so that the equivalent dipole length $D = \mathcal{I}\,\sigma/6$, Eq. (8a), remains smaller than the characteristic trap length. We adapt the asymptotic model with universal nodal lines to the calculation of the trap energy levels in the presence of both dipole-dipole and short-range interactions. Finally, in Sec. III C, we show that there is a close connection between cold collisions in free space as discussed in Sec. III A and collisions in an isotropic harmonic trap presented in Sec. III B. To this end, we relate the energy shift of the $\ell = 1$ trap levels to the scattering volume.

A. Free particles or weak confinement

We first consider confinement of the colliding particles that is so weak that it can, to a good approximation, be neglected altogether. When using the asymptotic model with universal nodal lines, a given pair of colliding atoms is characterized by its field-free s-wave scattering length a or, equivalently, by the nodal parameter x_{00}, i.e., a node position of the corresponding field-free s-wave threshold wave function [25]. This approach is easily generalized to account for the presence of nonresonant light with intensity $\mathcal{I}$ for both s-wave [18] and p-wave collisions (cf. Paper I [29]), where a, respectively x_{00}, determines the colliding species. A general picture of the behavior of the scattering volume as a function of the nonresonant light intensity for all pairs of particles is thus obtained in terms of a contour plot, as shown in Fig. 1 for a single-channel calculation with $\ell = 1$. The range chosen for x_{00} corresponds to one quasiperiod of the field-free s-wave scattering length varying from $-\infty$ to $+\infty$; cf. Paper I [29]. Two singularities are observed in Fig. 1 for $m = 0$ and one for $|m| = 1$. These are indicated by the thick red lines and correspond to infinitely strong interactions between the colliding particles. For $m = 0$ and a nodal parameter $0.1495\,\text{r.u.} \leqslant x_{00} \leqslant 0.1505\,\text{r.u.}$ (corresponding to a field-free s-wave scattering length in the range 0.9724–1.414 r.u.), less than about 2 r.u. or $2\,\text{GW/cm}^2$ of

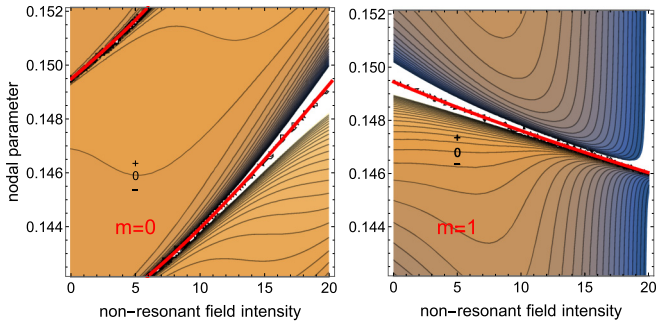

FIG. 1. Scattering volume as a function of the nonresonant field intensity $\mathcal{I}$ and the nodal parameter x_{00} for $m = 0$ (left) and $m = 1$ (right) in a single-channel calculation ($\ell = 1$). The gray contour lines vary in 40 steps between -150 and 150 for $m = 0$ and -2 and 2 for $m = 1$ with the zero line labeled and the plus and minus signs indicating the regions of positive and negative values of the scattering volume. The red thick lines indicate the values of $\mathcal{I}$ and x_{00} for which the field-dressed scattering volume diverges. Note that the absolute value of the scattering volume is in general much larger for $m = 0$ than for $|m| = 1$, and that the width of the divergences is generally also much larger, increasing with the light intensity for $m = 0$, while decreasing for $|m| = 1$. Reduced units (r.u.) are used.

nonresonant light intensity is sufficient to effectuate a huge change of the scattering volume. Such an s-wave scattering length is found for a mixture of ^{7}Li and ^{40}K, colliding in the lowest triplet state. Similarly, for $|m| = 1$, the lowest intensities to realize a divergence of the scattering volume are needed for species characterized by a nodal parameter $0.1490\,\text{r.u.} \leqslant x_{00} \leqslant 0.1495$ r.u. or, respectively, a field-free s-wave scattering length in the range 0.8428–0.9724 r.u., such as the interspecies triplet scattering length of ^{41}K and ^{87}Rb [52].

The picture in Fig. 1 is only of illustrative character due to the single-channel approximation. A more quantitative picture is obtained in multichannel calculations. Figure 2 shows, for $n = 9$ coupled channels, the singularities of the scattering volume as a function of the nonresonant light intensity and the field-free s-wave scattering length (bottom), respectively the nodal parameter (top). The left- and right-hand sides of Fig. 2 correspond to $m = 0$ and $|m| = 1$, respectively. For simplicity, only the singularities (corresponding to the red thick lines in Fig. 1) are shown and the contours are omitted. The bound states, whose occurrence at threshold causes the singularity, are labeled by $\widetilde{\ell}$, in reference to the ℓ channel with the largest weight in the field-dressed wave function. For the lowest two values, $\widetilde{\ell} = 1$ and $\widetilde{\ell} = 3$, the singularity curves vary rapidly and almost linearly as a function of the nonresonant light intensity $\mathcal{I}$, especially for $\widetilde{\ell} = 1$ and $m = 0$ (left part of Fig. 2), where a very broad anticrossing between the $\widetilde{\ell} = 1$ and $\widetilde{\ell} = 3$ singularity curves occurs for $\mathcal{I} \sim 10$ r.u. In this case, the occurrence of a bound level at threshold depends only to a limited extent on the s-wave scattering length. Rather, it is essentially determined by the nonresonant field intensity, i.e., the anisotropic long-range interaction. For $\ell = 1$, $|m| = 1$ (top right part of Fig. 2), a negative slope of the singularity curve is observed at low intensity. This is caused by the repulsive character of the effective adiabatic potential; cf. Table I in Paper I [29]. The large differences between the single-channel results (Fig. 1, right part) and multichannel results for $\mathcal{I} > 10$ r.u. (Fig. 2, right upper panel) are due to the coupling between ℓ partial waves. For an intensity higher than about 10 r.u., the coupling of the $\ell = 1$ channel with the other ones becomes dominant, turning the slope of the singularity curve positive, as for all the other (ℓ, m) values.

For the larger values of $\widetilde{\ell}$, singularities appear for a field-free s-wave scattering length approximately equal to zero (or, equivalently, $x_{00} = 0.149481$ r.u.), for $\widetilde{\ell} = 5$, 9, 13, and approximately equal to 0.96 r.u. (resp., $x_{00} = 0.144652$ r.u.) for $\widetilde{\ell} = 7$, 11, 15 [1]. These two values of the field-free s-wave scattering length are close to those predicted by the analytical model of Gao [53]. The corresponding singularity curves of the p-wave scattering volume vary only slowly with the light intensity. This indicates that the corresponding field-dressed wave functions strongly depend on the short-range interaction and almost not on the anisotropic long-range interaction. It can be understood in terms of the height of the rotational barrier which, being proportional to $\propto \ell^3$, increases rapidly with ℓ and is barely modified by the nonresonant light at the studied intensities.

In the single-channel approximation, the width of the singularity as a function of either x_{00} or $\mathcal{I}$ can be deduced from the results of Fig. 1. Let us define by w the width of a singular function of the type $y(x) = w/(x - x_p)$ with a pole at $x = x_p$. Then, for instance, for $m = 0$ the width in $\mathcal{I}$ increases with light intensity from about 12 r.u. at the bottom of the figure up to about 220 r.u. at $\mathcal{I} = 20$ r.u., whereas for $|m| = 1$ it decreases from about 5.6 r.u. down to 0.5 r.u. at $\mathcal{I} = 20$ r.u. It is worth mentioning that the width of the singularity as a function of intensity is not independent of the width as a function x_{00}. At a given point in the $(\mathcal{I}, x_{00})$ plane, the width along the first axis is proportional to the width along the other one, with the proportionality factor being equal to the opposite of the slope of the singularity curve.

B. Strong confinement

If the pair of particles is confined in an isotropic 3D harmonic potential of frequency ω, a term $\beta_\omega^4 x^2$ has to be added in Eq. (4), describing the relative motion in van der Waals reduced units, with

$$\beta_\omega = \sigma\sqrt{\frac{\mu\omega}{\hbar}} = \sigma/a_\omega, \tag{11}$$

where a_ω (ϵ_ω) is the trap reduced unit of length (energy)

$$\epsilon_\omega = \hbar\omega = \frac{\hbar^2}{\mu(a_\omega)^2} = 2\epsilon(\beta_\omega)^2. \tag{12}$$

With the unit factors a_ω and ϵ_ω, the length x_ω (resp., energy e_ω) expressed in reduced units of the harmonic oscillator [r.u.(ω)] is related to the corresponding value x (resp., $\mathcal{E}$) in van der Waals reduced units (r.u.) by $x_\omega = x\beta_\omega$ [$e_\omega = \mathcal{E}/(2\beta_\omega^2)$]. When strongly confined in a trap, where at large distance the trapping potential $\propto x^2$ prevails, the particles will explore only

[1] Note that it is necessary to introduce the channel $\ell_{\max}$ (here $\ell_{\max} = 17$) to obtain converged results for the channels $\ell \leqslant \ell_{\max} - 2$.

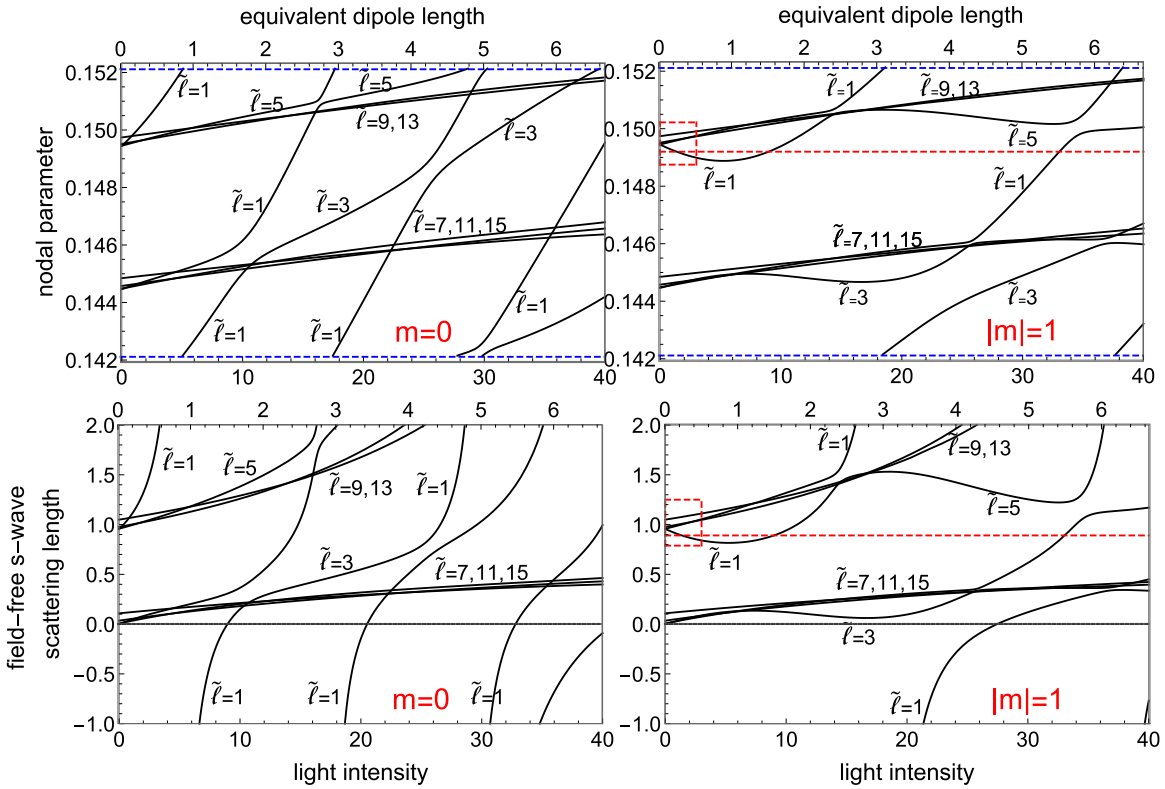

FIG. 2. Map of the singularities of the scattering volume (analogous to the red lines in Fig. 1) as a function of either the nodal parameter x_{00} in reduced units (top panels) or the field-free s-wave scattering length a in reduced units r.u. (bottom panels) and of the nonresonant light intensity in reduced units r.u., for $m = 0$ (left) and $|m| = 1$ (right). The scaling with the equivalent dipole length, D in Eq. (8a), for the anisotropic interaction is also shown in the top horizontal axis in each panel. The singularities are obtained in terms of the appearance of a zero-energy bound state and correspond to infinitely strong interaction between the particles. The calculations have been performed for odd ℓ values from 1 to 17 ($n = 9$ channels). The horizontal blue dashed lines in the top graphs indicate the values of the nodal parameter for which the field-free s-wave scattering length is infinite. The curves corresponding to $\widetilde{\ell} = 5, 9, 13$ (resp. $\widetilde{\ell} = 7, 11, 15$) are grouped in a roughly horizontal beam starting from an initial value of approximately $x_{00} \sim 0.15$ r.u. (resp., $x_{00} \sim 0.145$ r.u.) in the top graphs and from an initial value $a \sim 1$ r.u. (resp., $a \sim 0$ r.u.) in the bottom ones. The data within the red box are shown in more detail in Fig. 3, and the red dashed lines indicate the cases that will be examined in Figs. 4 and 5 ($x_{00} = 0.1492$ r.u., $a = 0.891$ r.u.).

a limited range of the dipole-dipole interaction potential. We thus may expect that, in the lowest positive-energy states of the trap, the behavior of the interparticle interaction will be close to the one described by small kx or, equivalently, by the threshold case, $k = 0$ (cf. Sec. II E of Paper I [29]), where k denotes the wave number in van der Waals reduced units ($\mathcal{E} = k^2$). Due to the trap, the spectrum possesses bound states only. The study of the asymptotic phase shift of the scattering wave functions is thus replaced by analysis of the bound-state energy shift with respect to the m-independent energy of the unperturbed trap states in harmonic oscillator reduced units, $e_\omega(N\ell) = (2N + \ell + 3/2)\,\mathrm{r.u.}(\omega)$ ($N \geqslant 0$ integer). We consider here only the case where a_ω is larger than σ and we limit the nonresonant light intensity to relatively small values, so that the characteristic length of the dipole-dipole interaction D remains always much smaller than a_ω.

To calculate the energy $\mathcal{E}$ of the bound states, we adapt the general procedure described in Ref. [25]. The wave function satisfies boundary conditions both on the nodal lines and at large distance $x_{\max}$. The initial condition for the inward integration of the particular solution $\mathbf{f}^\ell(\mathcal{E}, x)$ is given by $f^\ell_{\ell'}(\mathcal{E}, x_{\max}) = \delta_{\ell,\ell'} \exp(-\beta_\omega^2 x_{\max}^2/2)$ in the channels ℓ'. Writing the physical wave function $\mathbf{z}(\mathcal{E}, x)$ as a linear combination of the solutions $\mathbf{f}^\ell(\mathcal{E}, x)$ and requiring it to vanish on the nodal lines yields the quantization condition for the energy.

The intensity dependence of the bound-state energies, calculated with three odd ℓ values, $|m| = 1$, and a trap potential $\beta_\omega = 0.05$ (i.e., a trap length $a_\omega = 20\,\sigma$) is studied in two different intensity ranges. In both cases, the chosen nodal parameter is $x_{00} = 0.1492$ r.u. and the field-free s-wave scattering length is equal to 0.891 r.u. For this choice of parameters, an untrapped pair of particles subject to nonresonant light possesses two times a bound state with $\widetilde{\ell} = 1$, $|m| = 1$ at threshold, as shown in Fig. 2, for a light intensity $\mathcal{I}$ equal to 1.36 and 9.01 r.u. The corresponding equivalent dipole lengths D, cf. Eq. (8a), amount to $0.23\,\sigma$ and $1.50\,\sigma$, as shown in Fig. 2.

The intensity regions around $\mathcal{I} = 1.36$ and 9.01 r.u. are explored separately in Figs. 4 and 5. The relevant field-free $|m| = 1$ trap states correspond to $N = 0$, $\ell = 1$ [the lowest odd-ℓ trap level, with $e_\omega = 5/2\,\mathrm{r.u.}(\omega)$], $N = 0$, $\ell = 3$, and $N = 1$, $\ell = 1$ [the doublet of trap levels with $e_\omega = 9/2\,\mathrm{r.u.}(\omega)$] in Fig. 4 and the triplet of trap levels with $e_\omega = 13/2\,\mathrm{r.u.}(\omega)$, $N = 0$, $\ell = 5$, $N = 1$, $\ell = 3$, and $N = 2$, $\ell = 1$ in Fig. 5.

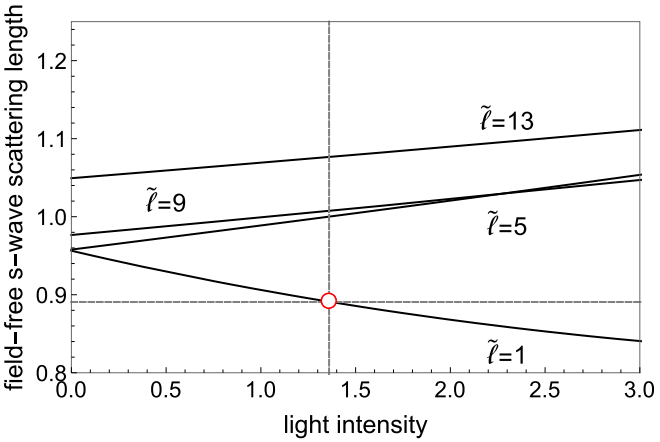

FIG. 3. Inset of the bottom right part of Fig. 2, i.e., map of the singularities of the scattering volume as a function of the field-free s-wave scattering length (in r.u.) and nonresonant light intensity (in r.u.) for $|m| = 1$. Horizontal gray line: field-free s-wave scattering length equal to 0.891 r.u. (corresponding to $x_{00} = 0.1492$ r.u.), the value used in Figs. 4 and 5; vertical gray line: predicted value of the position of the singularity (the red circle simply marks their intersection).

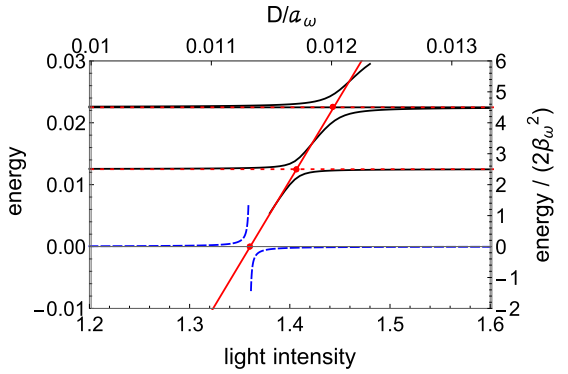

FIG. 4. Trap state energy as a function of the nonresonant light intensity $\mathcal{I}$ (black lines), compared to the energy of the field-free trap states (red dashed lines), identified in the text. The scales are reduced units (r.u.) of the van der Waals interaction (left), reduced units [r.u.(ω)] of the harmonic oscillator (right), nonresonant light intensity (in r.u.) (bottom), and ratio of the equivalent dipole length D, Eq. (8a), to harmonic oscillator length a_ω (top). The light-induced anticrossings of the field-free $\ell = 1$ trap states with the intensity-dependent last bound p-state (for negative energies), respectively p-wave shape resonance (for positive energies) for untrapped particles (red solid line), are clearly observable. The calculation is performed for $\beta_\omega = 0.05$ in a three-channel model with $\ell = 1$, 3, 5, $|m| = 1$ with $x_{00} = 0.1492$ r.u., i.e., a field-free s-wave scattering length of 0.891 r.u. This intensity range corresponds to the first intersection of the red dashed horizontal line in Fig. 2 with the black $\tilde{\ell} = 1$ curve. The blue dashed line displays the intensity dependence of the scattering volume, calculated under the same conditions ($\ell = 1$, 3, 5, $|m| = 1$, and $x_{00} = 0.1492$ r.u. but $\beta_\omega = 0$) and multiplied for convenience by the factor B (for $N = 0$) of Table III in Appendix A.

Two avoided crossings are observed in Fig. 4, around $\mathcal{I} = 1.4$ and 1.43 r.u. They are due to the strong coupling that the anisotropic interaction induces between each of the two $\ell = 1$ trap states (with $N = 0$ and $N = 1$) and the untrapped last bound $\tilde{\ell} = 1$ state together with its continuation as a $\tilde{\ell} = 1$ shape resonance. The $N = 0$, $\ell = 3$ trap state is not noticeably perturbed; see the essentially horizontal black line in Fig. 4. The red curve displaying, for the untrapped pair, the intensity dependence of the energy of the last molecular p state (for negative energy) and of the p-wave shape resonance (for positive energy) crosses the red dashed curves representing the field-free $\ell = 1$ trap states at the position of the anticrossings. In addition, the red curve crosses the zero energy for the intensity at which the scattering volume diverges. The increase of the energy of the lowest bound p state with $\mathcal{I}$ in Fig. 4 is related to the repulsive character of the anisotropic interaction in the $\ell = 1$, $|m| = 1$ channel, as discussed in the previous subsection and visible in the negative slope of the $\tilde{\ell} = 1$ curve at small $\mathcal{I}$ in Figs. 2 and 3.

In Fig. 5, the situation is similar to that in Fig. 4, but the repulsive character of the dipolar interaction in the $\ell = 1$, $|m| = 1$ channel is superseded by the coupling with the other channels. As a consequence, and as is most generally the case, close to the divergence of the scattering volume, the energy of the lowest bound p state decreases with intensity in Fig. 5, and the slope of the singularity curve with $\tilde{\ell} = 1$ in Fig. 2 is positive near $\mathcal{I} = 9$ r.u. Note that while the $N = 1$, $\ell = 3$ and $N = 0$, $\ell = 5$ trap states (black solid lines showing avoided crossings in Fig. 5) are strongly mixed together in the vicinity of the divergence of the scattering volume, they are not noticeably mixed with the $N = 2$, $\ell = 1$ state (horizontal black lines at $e_\omega = 13/2$ r.u.(ω) in Fig. 5). The intensity dependence of the trap state energies in Fig. 5 is similar to the dependence of the energy of two aligned identical bosonic dipoles colliding in s wave under external confinement with strength characterized by D/a_ω [54], where D is the equivalent dipole length of Eq. (5a). Figure 2 of Ref. [54] shows the energy of lowest trapped state of the pair to dive down to negative energy close to the D/a_ω value at which the two-body potential supports a new bound state. Moreover, the same behavior is also predicted for identical fermions undergoing p-wave collisions [55].

Our calculations suggest that it should be possible to control the formation of molecular bound states in p-wave collisions by nonresonant light. This would be analogous to

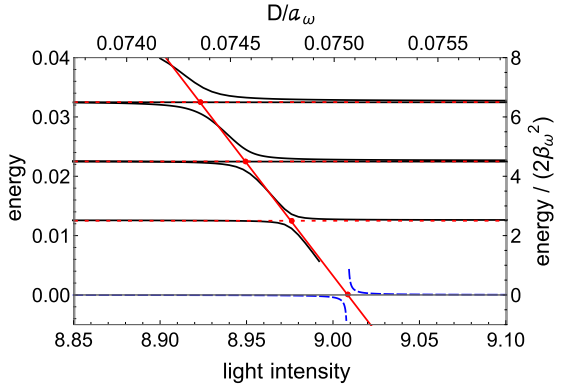

FIG. 5. Same as Fig. 4 but for the second intersection of the red dashed horizontal line (at $x_{00} = 0.1492$ r.u.) in Fig. 2 with the black $\tilde{\ell} = 1$ curve.

using nonresonant light to create molecules from bosonic atoms in *s*-wave collisions, as discussed in Ref. [16]: Slowly increasing the light intensity around $\mathcal{I} = 9.01$ r.u. would transfer the particle pair at resonance from the lowest trap state to the last molecular bound state. The same is true for the situation depicted in Fig. 4, except that the intensity has to be decreased around $\mathcal{I} = 1.36$ r.u. The inverse process consisting of climbing the trap ladder upward by a rapid variation of the light intensity would also be possible. Making molecules with nonresonant light this way would be a generalization of an experiment carried out for *s*-wave collisions, in the vicinity of a Feshbach resonance, of fermionic ^{40}K atoms in various hyperfine states confined in an optical three-dimensional (3D) lattice [56]. Note that the experimental results of Ref. [56] are reproduced by a model, also used below, describing the short-range interaction by a pseudopotential with a scattering length independent of energy [55,57,58]. Moreover, just as the scattering behavior discussed above can be tuned with either nonresonant light or dipole interaction strength, the formation of molecules also has its analog for colliding dipoles. Specifically, the simultaneous variation of the lowest trap state energy (black curve) and the scattering volume (blue dashed curve) with the nonresonant light intensity in Fig. 5 is reminiscent of the dependence of energy and scattering parameter on dipole coupling strength in Refs. [59,60]. In both cases, the effective interaction is increasingly attractive and the scattering parameter negative at the left of the resonance. Conversely, the interaction is decreasingly repulsive and the scattering parameter positive to the right of the resonance. In both cases, at resonance, the pair is transferred from the lowest trap state to the last molecular bound state. The main difference lies in the existence, in the case of nonresonant light control, of a small shift of the pole of the scattering volume relative to the position of the lowest anticrossing of the trap energies. This shift comes from the finite slope of the energy as a function of intensity, cf. the red curve in Fig. 5, which is due to the presence of the van der Waals potential and the energy, ℓ, and intensity dependences of the nodal lines.

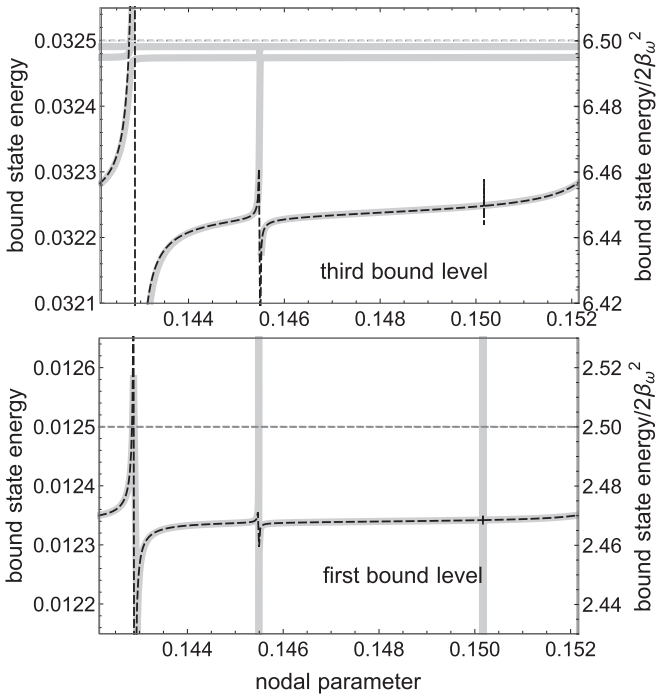

FIG. 6. Trap state energy (thick gray curves) of $m = 0$ states as a function of the nodal parameter x_{00} for $\mathcal{I} = 6$ r.u. and $\beta_\omega = 0.05$, in van der Waals reduced units on the left-hand side and in harmonic oscillator reduced units on the right-hand side for the lowest state of the trap with $N = 0$, $\ell = 1$ (bottom), and the third state, i.e., the set of states with $2N + \ell = 5$, whose threefold degeneracy is removed by the dipolar interaction (top). The black dashed lines display the x_{00} dependence of the field-dressed scattering volume $\mathcal{M}_0$ of untrapped particles, multiplied by $B = 1.35510^{-6}$ r.u. ($B = 5.910^{-6}$ r.u.) and vertically shifted by 0.01233850 r.u. (0.03223315 r.u.), to fit the scale of the figure. This corresponds to a global shift of $A = -0.0001615$ r.u. ($A = -0.00026685$ r.u.) of the first (third) trap state. The interaction-free trap states are indicated by the thin dashed gray lines. The calculations are performed in a three-channel model ($\ell = 1, 3, 5$). Reduced units r.u. are used.

C. Connecting *p*-wave scattering control with nonresonant light in weak and strong confinement

For a pair of trapped particles subject to nonresonant light, it is possible to connect the intensity dependence of the *p*-wave scattering properties in the weak and strong confinement case by studying the intensity dependence of either the field-dressed scattering volume $\mathcal{M}_0$ or the trap state energy shifts. As discussed in detail in Sec. III of Paper I [29], the field-dressed scattering volume, $\mathcal{M}_0$, depends on the nodal parameter x_{00} that is characteristic of the short-range interactions in the field-free untrapped pair and displays singularities, i.e., signatures of the appearance of $\widetilde{\ell}$-bound states at threshold. Moreover, for a given intensity, many singularities (for different $\widetilde{\ell}$) are found, cf. Fig. 2, whereas for a given nodal parameter, i.e., for a given choice of particles, intensity intervals that contain divergences have to be carefully selected. So we first examine the x_{00} dependence of the trap state energy shifts for a fixed light intensity $\mathcal{I}$.

Without any interaction in the pair, the trap energy for a state with quantum numbers N, $\ell = 1$, m is given by $\mathcal{E}(N\ell m) = 2(\beta_\omega)^2(2N + \ell + 3/2)$ r.u. in van der Waals reduced units or, equivalently, $e_\omega(N\ell m) = (2N + \ell + 3/2)$ r.u.(ω), in harmonic oscillator reduced units. The interparticle interaction in the untrapped pair induces a shift $\Delta\mathcal{E}_{N,\ell=1,m}$ that will depend on the characteristics of this interaction, i.e., the short-range interactions described by the nodal parameter x_{00} (or equivalently the field-free scattering length), the van der Waals asymptotic interaction $-1/x^6$ in reduced units, and the anisotropic dipolar interaction induced by the light.

Figures 6 and 7 display x_{00} dependence of the energy of the first (the lowest) and third trap state for a nonresonant light intensity of $\mathcal{I} = 6$ r.u. ($D = \sigma$) and a trapping potential with $\beta_\omega = 0.05$ ($a_\omega = 20\sigma$). $m = 0$ in Fig. 6 and $|m| = 1$ in Fig. 7. As everywhere in this paper, the x_{00} range is chosen so that the corresponding field-free *s*-wave scattering length varies once from $-\infty$ to $+\infty$. Note that the lowest trap state is nondegenerate, whereas the third one is triply degenerate. The short-range interaction of the particles and the coupling to the nonresonant light produce an ℓ-dependent energy shift

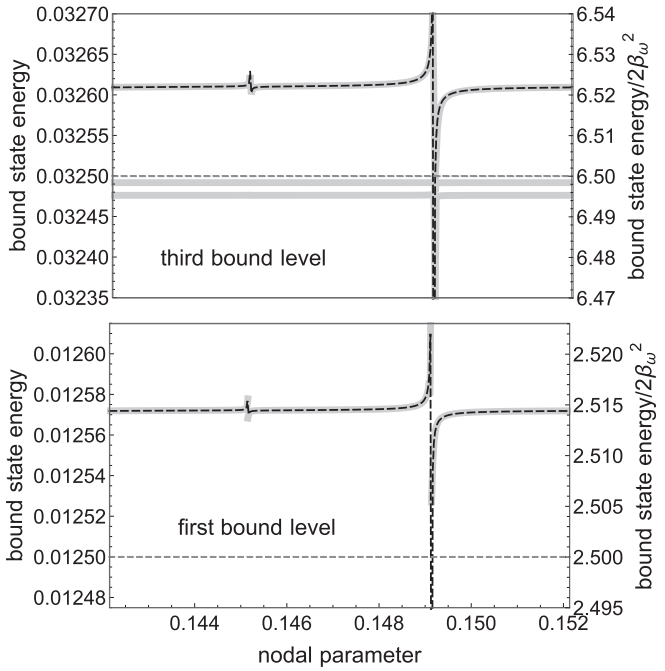

FIG. 7. Same as Fig 6, but for $|m| = 1$ states. The scaling parameters for $\mathcal{M}_0$ are $B = 1.5 \times 10^{-6}$ r.u. ($B = 5.9 \times 10^{-6}$ r.u.) and shifts of 0.0125725 r.u. (0.032611 r.u.), corresponding to a global shift of $A = 0.0000725$ r.u. (resp. $A = 0.000111$ r.u.), of the first (third) state. Reduced units (r.u.) are used.

that removes the degeneracy. Therefore, three separate gray curves are observed in the top of Figs. 6 and 7. In the lowest $\widetilde{\ell} = 1$ adiabatic potential, $V_{\ell=1}(x) \sim -c_3/x^3$, the interaction is attractive with $c_3 > 0$ for $m = 0$ (resp. repulsive with $c_3 < 0$ for $|m| = 1$), and the trap state energy is shifted toward lower (resp. higher) energy; cf. the difference between the thin dashed gray lines corresponding to pure trap state and the thick gray curve associated with the $\widetilde{\ell} = 1$ perturbed p-trap state. This difference is essentially constant, except close to a divergence. The adiabatic potentials $\widetilde{\ell} \geqslant 3$ are all attractive, resulting in a negative energy shift of the trapped states $\widetilde{\ell} = 3$ and 5. The $\widetilde{\ell} = 1$ trap states show an x_{00} dependence of their energy in the vicinity of the unperturbed trap state energy that is quite similar to that of the field-dressed scattering volume $\mathcal{M}_0^m(x_{00})$. To visualize this in Figs. 6 and 7, we have scaled the x_{00} dependence of the field-dressed scattering volume shown in Fig. 2 of Paper I [29] to fit the energy range of the trap states and included the resulting curves with black dashed lines. The three resonances of $\mathcal{M}_0^m(x_{00})$ observed in Fig. 6 for $m = 0$, which are associated to the channels $\ell = 1$, 3, and 5, appear at exactly the x_{00} value as those of the trap state energies. The same is true for the $|m| = 1$ resonances in Fig. 7, except that the resonance with $\ell = 5$, which is extremely narrow, is not resolved in our calculations.

The ease with which the numerical results for the energies in the trapped case and the scattering volume in the case of free collisions in Figs. 6 and 7 can be connected suggests a closer inspection of their relation. The x_{00} dependence of the field-dressed scattering volume $\mathcal{M}_0^m(x_{00})$ was deduced in Sec. III A of Paper I [29]. Since it was only necessary to scale and shift $\mathcal{M}_0^m(x_{00})$ in order to display it together with the trap state energy shifts as a function of x_{00}, the simple ansatz for the interaction-induced shift in energy,

$$\Delta\mathcal{E}_{N,\ell=1,m}(x_{00}) = A + B\mathcal{M}_0^m(x_{00}), \tag{13}$$

should be sufficient. The linear equation (13) is written for BC2 reference functions, cf. Table I in Paper I [29], and assuming that $\Delta\mathcal{E}_{N,\ell=1,m} \ll 4(\beta_\omega)^2$, i.e., the energy shift is much smaller than the level spacing of interaction-free trap levels. In Eq. (13), the parameters A and B depend on the confinement β_ω and on the quantum numbers N, ℓ, and m, but are independent of the nodal parameter. For the lowest trap level, i.e., $N = 0$, $\ell = 1$, it is possible to determine this dependence. To this end, we calculate the energy related to the trap potential for a wave function, $f_{\rm pert}(x)$, which, for $\beta_\omega x \ll 1$, has the same behavior as the untrapped threshold p-wave function $u(x)$. While the trap wave function without any interaction is proportional to $x^2 \exp[-(\beta_\omega x)^2/2]$, in the presence of interactions the ansatz $f_{\rm pert}(x) = u(x)\exp[-(\beta_\omega x)^2/2] = [x^2 - ax - b - c\ln(x)/x - d/x - \mathcal{M}_0/x]\exp[-(\beta_\omega x)^2/2]$ ensures the correct behavior at long interparticle distances. In this ansatz, a, b, ... (cf. Eqs. (A7) and (A8) of Paper I [29]) depend on the m- and $\mathcal{I}$-dependent parameters c_3, c_4, ..., which describe the asymptotic form of the effective potential for p waves, cf. Table I of Paper I [29], while $u(x)$ is reported in Eq. (B7) of Paper I [29]. With this ansatz, the mean trap potential energy becomes

$$V_{\rm pert} = \frac{\int \beta_\omega^4 x^2 f_{\rm pert}(x)^2 dx}{\int f_{\rm pert}(x)^2 dx}, \tag{14}$$

where the integration runs from a small value to ∞. Using the virial theorem for the harmonic oscillator, the total energy is twice this value. Comparing the total energy of the trapped interacting pair to the trap level without interaction, we find, for the lowest trap level,

$$A = -\frac{4c_3}{3\sqrt{\pi}}\beta_\omega^3, \quad B = \frac{8}{\sqrt{\pi}}\beta_\omega^5. \tag{15}$$

This is in good agreement with the numerical results that were obtained for $m = 0$ and $m = \pm 1$ in both single-channel ($\ell = 1$) and multichannel ($\ell = 1$, 3, 5) calculations. For instance, the estimates of A and B for the lowest $m = 0$ state shown in Fig. 6 are 1.41×10^{-6} r.u. and -1.504×10^{-4} r.u., to be compared with the values quoted in Fig. 6, i.e., 1.355×10^{-6} r.u. and -1.615×10^{-4} r.u.. Similarly, for $|m| = 1$, i.e., Fig. 7, the estimates for A and B are 1.41×10^{-6} r.u. and 7.523×10^{-5} r.u., to be compared to 1.5×10^{-6} r.u. and 7.25×10^{-5} r.u.

This method is, however, not suitable to determine A and B for higher trap states, since the ansatz $f_{\rm pert}(x)$ is built upon the (zero-energy) threshold wave function $u(x)$. We therefore resort to a more general procedure described in detail in Appendix A. The parameter A is obtained from first-order corrections to the energy of trap states due to the asymptotic potential. For the evaluation of parameter B, the energy shift of $\ell = 1$ states, equal to $B\mathcal{M}_0^m(x_{00})$, is obtained to first order in a model where the short-range interactions are accounted for by a contact potential and the energy of the perturbed trapped states is evaluated analytically [54,55,57,58]. The close connection between the cases of weak (or no) and strong

confinement is thus explained by the important role of the short-range interactions.

IV. SCATTERING VOLUME AND ORIENTATION OF THE INTERPARTICLE AXIS

We study in the following the interdependence of the scattering volume and the orientation of the interparticle axis relative to the direction of the two dipoles induced by the nonresonant light. Remember that the dipoles are aligned along the polarization of the light, the laboratory Z axis; cf. Sec. II A. Our focus is on the orientation of the interparticle axis relative to the direction of the dipoles. Particular attention is paid to the case where the nonresonant light is used to induce a divergence of the scattering volume. We recall that this problem is formally identical to the case of permanent dipoles, provided their direction is fixed. While it is challenging to solve the complete scattering dynamics, insight can already be gained by examining the orientation as a function of interparticle distance.

Because of the symmetry of the problem, the representation of the Hamiltonian in the basis of the spherical harmonics is block diagonal in m and depends on the absolute value of m only. In an experiment, it is impossible to select a given value of m (except for very specific cases, such as samples in the shape of a pancake or a needle). Therefore, in general, the scattering states are a linear combination of two solutions, one with $m = 0$ and one with $m = \pm 1$. There is no mixing between the two m solutions but these solutions evolve differently as a function of the interparticle distance. This results in a variation of the orientation in the (x, z) or (y, z) plane of the interparticle axis with respect to the dipole direction. The orientation will thus in general be a function of the interparticle distance.

We distinguish below between freely movable and geometrically confined particles, the orientation of the dipoles being always fixed. For freely movable particles, we first inspect a single-channel model in Sec. IV A and generalize to the multichannel case in Sec. IV B. The situation of particles that are geometrically confined due to a specific shape of the trap giving rise for instance to quasi-2D or 1D samples is discussed in Sec. IV C.

A. Orientation of the interparticle axis at short internuclear distance: Single ℓ value

We start with the single-channel approximation (with $\ell = 1$) because of its simplicity and in order to gain some first intuition. Because of the symmetry around the laboratory fixed Z axis, it is sufficient to analyze the wave function in the Z-X plane ($\phi = 0$). This reduces the angular part to its dependence on θ, the angle between the interparticle axis and the laboratory fixed Z axis. The p-wave single-channel threshold wave function with mixed m character can thus be written as

$$\phi(x, \theta) = \cos(\alpha) u_0(x) \cos(\theta) + \sin(\alpha) u_1(x) \sin(\theta), \quad (16)$$

where $u_0(x)$ and $u_1(x)$ are threshold radial components of the eigenfunctions of the two blocks

$$H_m = \langle Y_{\ell=1,m} | H | Y_{\ell'=1,m} \rangle, \quad (17)$$

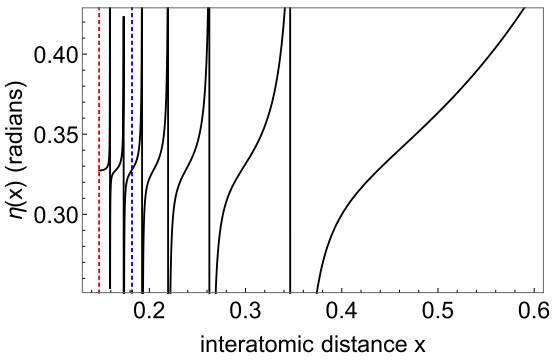

FIG. 8. Dependence of the angle $\eta(x)$, characterizing the main orientation of the interparticle axis with respect to the field direction, on interparticle distance x (in reduced units) for $\mathcal{I} = 6$ r.u. and $x_{00} = 0.148$ r.u. (which corresponds to an s-wave scattering length of 0.651 r.u.). The vertical red dotted line indicates the position of the repulsive wall $x_0(\mathcal{E} = 0, \ell = 1, \mathcal{I})$ (see text) and the blue one the position of the value of x chosen in Fig. 9. The asymptotic value of $\eta(x)$ in this example is $\pi/4$. Calculations are performed in the single-channel p-wave model.

with $m = 0$ and 1. They have the same asymptotic form $u_{|m|}(x) \equiv x^2 + \ldots$; cf. Paper I [29]. The angle α denotes the orientation of the dipole moments relative to the interparticle axis. More specifically, α determines the main orientation of the interparticle axis at large distance, where $u_0(x)$ and $u_1(x)$ are taken to be identical and equal to x^2. One can separate the function $\phi(x, \theta)$ into a radial part which depends only on the interparticle distance x and is asymptotically equal to x^2 and an angular part,

$$\begin{aligned}\phi(x, \theta) &= [\cos(\alpha)^2 u_0(x)^2 + \sin(\alpha)^2 u_1(x)^2]^{1/2} \\ &\quad \times \frac{\cos(\alpha) u_0(x) \cos(\theta) + \sin(\alpha) u_1(x) \sin(\theta)}{[\cos(\alpha)^2 u_0(x)^2 + \sin(\alpha)^2 u_1(x)^2]^{1/2}} \\ &= [\cos(\alpha)^2 u_0(x)^2 + \sin(\alpha)^2 u_1(x)^2]^{1/2} \\ &\quad \times \cos[\theta - \eta(x)], \end{aligned} \quad (18a)$$

where

$$\tan[\eta(x)] = u_1(x)/u_0(x) \times \tan(\alpha). \quad (18b)$$

For a fixed interparticle distance x, the angle $\eta(x)$ is the angle for which the wave function presents the maximum probability, i.e., it corresponds to the main orientation of the interparticle axis. In the asymptotic domain where $u_1(x)/u_0(x)$ is almost constant, $\eta(x)$ varies slowly and converges regularly toward its limit α. In contrast, at short distance ($x < 0.5$ r.u.) where the attractive $-1/x^6$ potential dominates and the radial functions $u_{m=0,\pm1}(x)$ are highly oscillatory, $\eta(x)$ changes rapidly. This is illustrated in Fig. 8, which displays η as a function of interparticle distance x. As x is decreased and approaches the nodal line, $\eta(x)$ approaches a value that depends on α and x_{00}, apart from sudden variations at the nodes of the wave function. This value amounts to ~0.33 radians in the example of Fig. 8.

The short-range behavior of $\eta(x)$ is further analyzed in Fig. 9, which shows the dependence of $\eta(x_{00} + \delta_x)$ on the nodal parameter x_{00} for various values of the asymptotic angle $\eta(x_{\max}) = \alpha$ (evaluated here at $x_{\max} = 200$ r.u.), with α

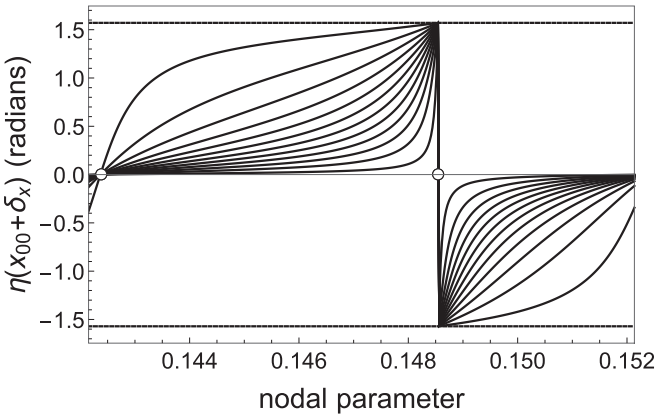

FIG. 9. Angle $\eta(x_{00}+\delta_x)$, characterizing the main orientation of the inter-particle axis with respect to the field direction at short distance, as a function of the nodal parameter x_{00} (in reduced units) for various values of the angle $\eta(x_{\max})=\alpha$ at large distance ($x_{\max}=200$ r.u.), with α varying from $\pi/24$ to $11\pi/24$. The intensity is $\mathcal{I}=6$ r.u. and the value of δ_x, $\delta_x=0.034$ r.u., is chosen such that $x_{00}+\delta_x$ is small and does not coincide with a node of the wave functions $u_m(x)$. For a nodal parameter corresponding to a bound state at threshold with either $m=0$ or $|m|=1$, $\eta(x_{00}+\delta_x)$ is independent on the asymptotic orientation α and is equal to either 0 or $\pm\pi/2$. The two small open circles indicate the corresponding positions of the divergences of the scattering volume for $m=0$ (left) and $|m|=1$ (right). Calculations are performed in the single-channel p-wave model.

varying from $\pi/24$ to $11\pi/24$. The value of δ_x is chosen such that $x_{00}+\delta_x$ is small and does not coincide with a node of the $u_{0,\pm1}(x)$ wave functions. The two constant cases correspond to $\alpha=0$ and $\alpha=\pi/2$. The short-range dependence of $\eta(x)$ on x_{00} can also obtained by calculating the slopes $D_m(x_0)=u'_m(x_0)$ of the two solutions at the position of their energy-, intensity-, and ℓ-dependent node $x_0(\mathcal{E},\ell,\mathcal{I})$ with $\ell=1$ and $\mathcal{E}=0$. This is explained in Appendix B. A remarkable observation can be made in the case when the scattering volume diverges, with the corresponding values of x_{00} indicated by the open circles in Fig. 9. Then $\eta(x_{00}+\delta_x)$ takes the same value, independent of its asymptotic value α, as is evident from all curves in Fig. 9 coinciding. This is in contrast to the case when the scattering volume remains finite, in which case the short-range value of η does depend on the asymptotic value. Next, we will examine whether the special behavior of the orientation of the interparticle axis relative to the dipole moments in the case of a diverging scattering volume still appears when the coupling between different partial waves is properly accounted for.

B. Orientation of the interparticle axis at short internuclear distance: Several channels

To analyze the role of the scattering volume for the orientation of the interparticle axis in a multichannel treatment, we consider a given asymptotic orientation and look at the angular behavior of the corresponding wave function as x decreases. This approach is motivated by the fact that any actual situation can be described by a superposition of wave functions with given asymptotic behavior. We start from the

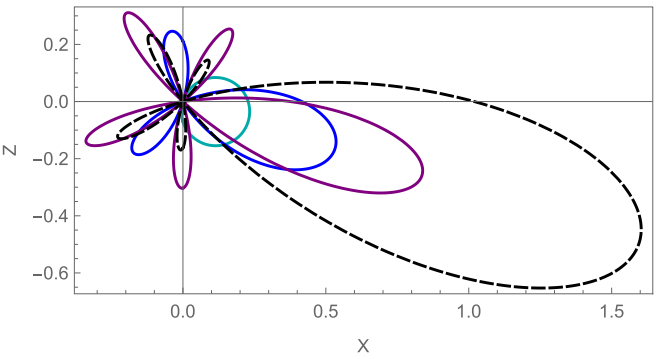

FIG. 10. Polar plot of the asymptotic wave function Eq. (20), for three channels with odd ℓ values, $\theta_0=-0.3\pi$ and $\phi=0$. Dashed black line: total wave function. Cyan, blue, and purple lines: partial wave functions with $\ell=1$, 3, and 5. Reduced units are used.

following general expression of the Dirac δ function:

$$\frac{\delta(\theta-\theta_0)}{\sin(\theta_0)}=\sum_{\ell=0}^{\infty}\sum_{m=-\ell}^{\ell}Y_{\ell,m}(\theta,\phi)Y^{\star}_{\ell,m}(\theta_0,\phi). \tag{19}$$

At large distance, the wave function providing the best representation of a given orientation θ_0 of the interparticle axis with respect to the laboratory fixed Z axis can be written as

$$f_{\rm asym}(\theta,\phi)=\sum_{\ell=\ell_{\min}}^{\ell_{\max}}\sum_{m=-\ell}^{\ell}Y_{\ell,m}(\theta,\phi)Y^{\star}_{\ell,m}(\theta_0,\phi). \tag{20}$$

We limit the sum over ℓ to odd values and restrict ϕ to zero due to symmetry, as in the previous subsection. Figure 10 shows the asymptotic wave function for the example of $\theta_0=-0.3\pi$, obtained by including in the calculation three values of ℓ and all corresponding m values. As expected, the wave function points towards -0.3π and, as also expected, higher ℓ waves would be required to properly describe the orientation.

To study the x dependence of the angular behavior of the wave function, we solve the Schrödinger equation for the three values of ℓ and all corresponding m values. We use the same method of inward integration as described in Paper I [29] and obtain a set of radial wave functions $u^m_{\ell,\ell'}(x)$, where ℓ denotes the channel associated to the physical solution and ℓ' refers to the channel in which the integration starts. At large distance, taken to be $x_{\max}$, the interaction between the different channels is small, and $u^m_{\ell,\ell'}(x_{\max})$ is taken as equal to a Kronecker $\delta_{\ell,\ell'}$. The complete wave function associated to given asymptotic conditions is thus given by

$$f(x,\theta,\phi)=\sum_{\ell=\ell_{\min}}^{\ell_{\max}}\sum_{\ell'=\ell_{\min}}^{\ell_{\max}}\sum_{m=-\ell}^{\ell}u^m_{\ell,\ell'}(x)\times Y_{\ell,m}(\theta,\phi)Y^{\star}_{\ell',m}(\theta_0,\phi), \tag{21}$$

where ℓ takes odd values only. We calculate separately the different ℓ components of the wave function,

$$f_\ell(x,\theta,\phi)=\sum_{\ell'=\ell_{\min}}^{\ell_{\max}}\sum_{m=-\ell}^{\ell}Y_{\ell,m}(\theta,\phi)Y^{\star}_{\ell',m}(\theta_0,\phi)u^m_{\ell,\ell'}(x), \tag{22}$$

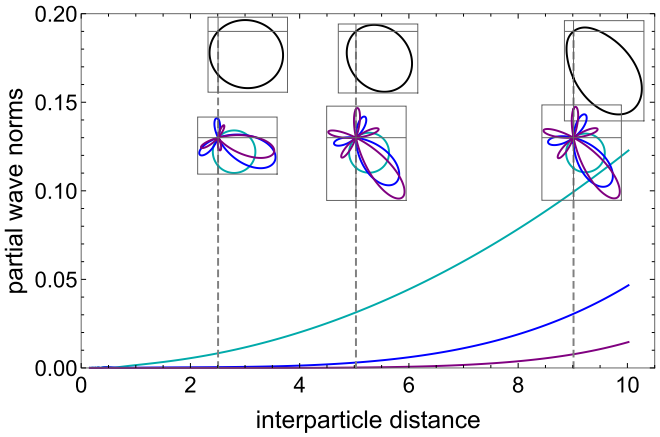

FIG. 11. Partial wave norms [cf. Eq. (23), cyan, blue, and purple curves for $\ell = 1, 3, 5$] as a function of interparticle distance x in r.u., for $\theta_0 = -0.3\pi$, $\mathcal{I} = 6$ r.u., and a nodal parameter that corresponds to a scattering volume far from the $\widetilde{\ell} = 1$ poles ($x_{00} = 0.147$ r.u. or, resp. $a = 0.494623$ r.u.). The insets show the angular behavior of the scattering wave function for several x whose positions are indicated by the vertical gray dashed lines. The angular behavior of the total wave function, Eq. (21), is depicted in black, at the top. The polar plots corresponding to the partial wave functions, Eq. (22), are also shown at the bottom. The asymptotic polar plot is shown in Fig. 10. For x smaller than about 2.5 r.u., the angle for which the probability is maximum becomes roughly fixed, with a value depending on the asymptotic orientation (here about $-\pi/4$). The calculation was performed with three values of ℓ and all corresponding m values.

and their norms,

$$N_\ell(x,\phi)^2 = \sum_{\ell'=\ell_{\min}}^{\ell_{\max}} \sum_{m=-\ell}^{\ell} \left| Y_{\ell',m}(\theta_0,\phi) u^m_{\ell,\ell'}(x) \right|^2. \qquad (23)$$

The functions u are the radial parts of the solutions that we calculate (with a separate calculation for each m) as an intermediate to the complete solution. Their number depends on m—for instance, in a three-channel calculation with $\ell = 1, 3, 5$, it is equal to 1 for $|m| = 5, 4$, equal to 2 for $|m| = 3, 2$, and equal to 3 for $|m| = 0, 1$.

In general, when the absolute value of the scattering volume is not too large, the partial wave functions are elongated according to the expected orientation at large distances and the evolution of the orientation with decreasing x does not present a spectacular behavior. This is illustrated in Fig. 11. The only notable point is that the orientation becomes fixed at short distance, with a direction that depends on the asymptotic orientation, just as in the single-channel case.

The situation is quite different when the scattering volume is close to one of its poles (for given $\widetilde{\ell}$, m), cf. Fig. 12 for two poles with $\ell = 1$. In this case, the partial wave norms, especially the one corresponding to the ℓ, m value of the pole, have a large maximum at short distance. Moreover, the orientation of the interparticle axis takes a fixed direction at short range, 0 or π for $m = 0$ and $\pm\pi/2$ for $|m| = 1$, not depending on the asymptotic orientation. In the first case, the dipoles are head to tail, whereas in the latter one, the interparticle axis becomes roughly perpendicular to the dipoles.

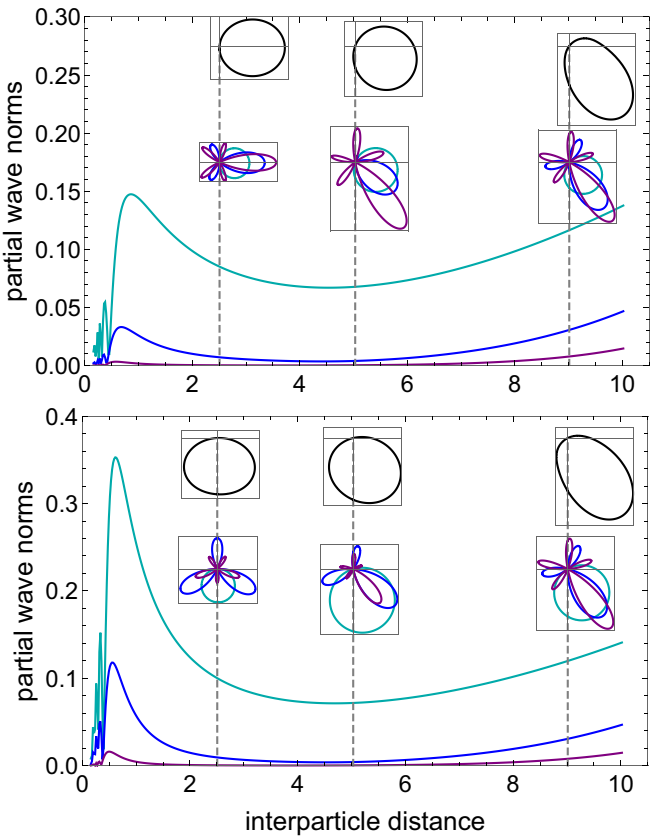

FIG. 12. Same as Fig. 11, but for a nodal parameter corresponding to a scattering volume close to a pole with $\widetilde{\ell} = 1$. Top: pole with $m = 0$, $x_{00} = 0.142906$ r.u. (s-wave scattering length $a = -1.31436$ r.u.), bottom: pole with $|m| = 1$, $x_{00} = 0.149140$ r.u. ($a = 0.87585$ r.u.). For x smaller than about 2.5 r.u., the angle for which the probability is maximum becomes more or less fixed, with the direction not depending on the asymptotic orientation (0 for the divergence with $m = 0$ and $-\pi/2$ for that with $|m| = 1$).

A similar behavior is observed for poles with other values of $\widetilde{\ell}$ but the resonance character of the wave function may become even more pronounced. This is illustrated in Fig. 13, which shows the example of a pole with $\widetilde{\ell} = 5$, $|m| = 1$. The main direction at short distance is $-\pi/2$ as for the pole $\widetilde{\ell} = 1$, $|m| = 1$; i.e., the dipoles are perpendicular to the interparticle axis. However, the relative importance of the partial waves is quite different and the maximum of the partial wave norms with a larger ℓ is higher and occurs at shorter distance, since the rotational barrier for $\ell = 5$ is higher and located at a smaller separation than the $\ell = 1$ barrier.

In conclusion, close to a singularity of the scattering volume, the main orientation at short interparticle distance is fixed, irrespective of the specific experimental conditions (such as pancake or needle-shaped samples). So controlling the scattering volume, either by tuning nonresonant light intensity or by choosing an effective dipole length for aligned permanent dipoles, does not only affect the interaction strength of the scattering partners but also their orientation. While this is expected for collisions of polar molecules, it is less obvious for scattering in the presence of nonresonant light.

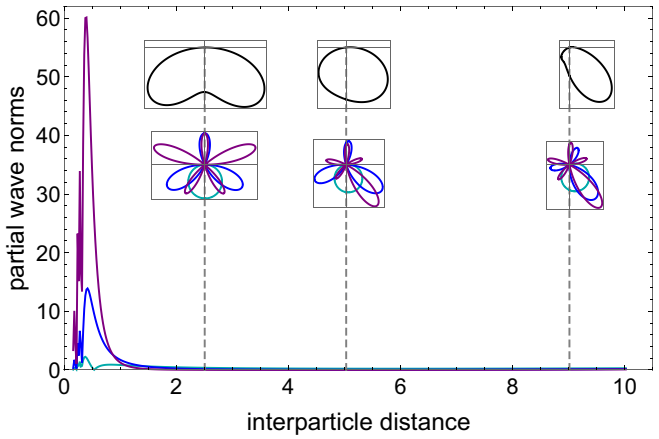

FIG. 13. Same as Fig. 11, but for a nodal parameter corresponding to a scattering volume close to a pole with $\widetilde{\ell} = 5$, $|m| = 1$ ($x_{00} = 0.150116$ r.u. or, resp., $a = 1.19953$ r.u.). For x smaller than about 2.5 r.u., the average angle θ becomes more or less fixed at a value close to $-\pi/2$, not depending on the asymptotic orientation.

C. Fixed orientation of the internuclear axis

We will now consider the situation where the direction of the interparticle axis is fixed by geometrical constraints due to the trap, such as those encountered in a disk or needle sample. For a given orientation α of the interparticle axis with respect to the common dipole direction, the Hamiltonian can be written as

$$H_\alpha = \cos^2(\alpha)\, H_0 + \sin^2(\alpha)\, H_1, \tag{24}$$

where the m-dependent block Hamiltonians H_m are defined in Eq. (17). Equation (24) results from the fact that there is no mixing between solutions with $m = 0$ and $m = \pm 1$. In a calculation accounting for n partial ℓ waves, H_α is a $n \times n$ matrix, and the diagonal matrix element for the p-wave channel is equal to

$$\frac{2}{x^2} - \frac{1}{x^6} - \mathcal{I}\frac{4\cos^2(\alpha) - 2\sin^2(\alpha)}{15x^3}. \tag{25}$$

We analyze the behavior of the field-dressed scattering volume for four different values of α in Fig. 14. These values correspond to the case of $m = 0$ and $|m| = 1$ states alone in Figs. 14(a) and 14(b), respectively, to an equal mixture of $m = 0$ and $|m| = 1$ states in Fig. 14(c), and to the case in Fig. 14(d), where $\alpha = \alpha_{QL}$ and the potential becomes quasi-long range (QL) [26]. In this latter case, $\cos^2(\alpha) = 1/3$, $\sin^2(\alpha) = 2/3$. This means that the $1/x^3$ term due to the nonresonant light (or dipole-dipole interaction) disappears from the diagonal term $\ell = 1$ of the Hamiltonian. The quasi-long-range character of the interaction obtained in this case is analogous to that in the problem of nonresonant light control of the s-wave scattering length for even-parity states [19].

Each panel in Fig. 14 displays essentially two divergences of the scattering volume, which can be labeled by $\widetilde{\ell} = 1$ and $\widetilde{\ell} = 3$. While this is expected in the cases in Figs. 14(a) and 14(b) where there is no m mixing, it is more surprising in the other cases. These divergences can in all cases be labeled by $\widetilde{\ell} = 1$ and $\widetilde{\ell} = 3$ (the $\widetilde{\ell} = 5$ divergences, too narrow, are not visible here). Note that the positions of the $\widetilde{\ell} = 1$ divergences vary notably with α: The $\widetilde{\ell} = 1$ resonances of the two pure cases (top part of Fig. 14) are located at very distant x_{00} values

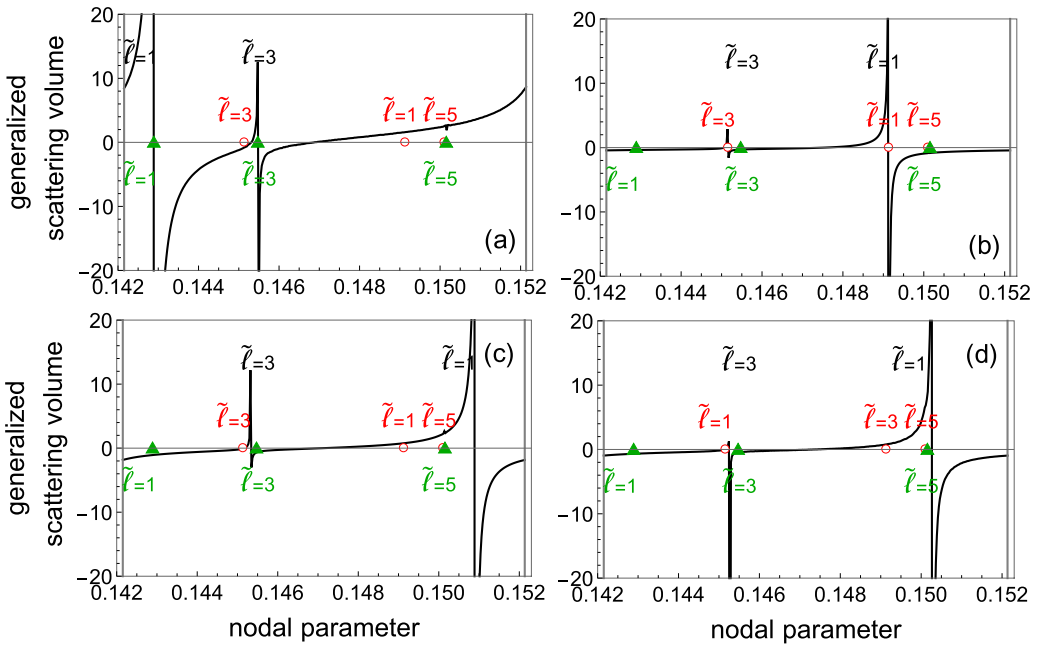

FIG. 14. Dependence of the field-dressed scattering volume (in r.u.) on the nodal parameter x_{00} (in r.u.) for a fixed orientation of the interparticle axis, with a fixed mixing of $m = 0$ and $m = \pm 1$ states characterized by the values of $\cos^2\alpha$ and $\sin^2\alpha$ in the Hamiltonian Eq. (24). (a) $\alpha = 0$, only $m = 0$; (b) $\alpha = \pi/2$, only $m = \pm 1$; (c) $\alpha = \pi/4$, equal mixing of the two values; (d) $\alpha = \alpha_{QL}$, with $[\cos^2(\alpha), \sin^2(\alpha)] = (1/3, 2/3)$. The red open circles (green triangles) indicate the divergence of the scattering volume for pure $m = 0$ ($|m| = 1$) states. The vertical gray lines indicate the x_{00} values corresponding to infinite field-free s-wave scattering length. The calculations are performed for three channels and $\mathcal{I} = 6$ r.u.

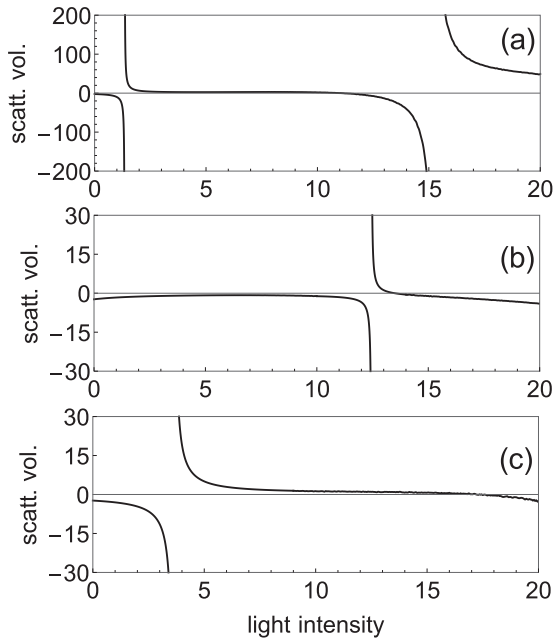

FIG. 15. Dependence of the field-dressed scattering volume on the light intensity $\mathcal{I}$ for a given orientation of the interparticle axis. (a) $\alpha = 0$, i.e., $m = 0$ alone; (b) $\alpha = \pi/2$, i.e., $m = \pm 1$; and (c) $\alpha = \pi/4$, equal mixing of $m = 0$ and $m = \pm 1$ states. The calculations are performed for $x_{00} = 0.15$ r.u., i.e., a field-free s-wave scattering length equal to 1.16 r.u. (for instance, ground triplet of $^{41}K^{87}Rb$ [25]), within a three-channel model. Reduced units (r.u.) are used.

so that the $\tilde{\ell} = 1$ pole for mixed m [in Fig. 14(c)] lies between the $m = 0$ pole and the $|m| = 1$ pole of the next interval of x_{00} values (remember the quasiperiodicity of the nodal line model with x_{00}). For $\widetilde{\ell} = 3$, the two "pure" poles are very close one to the other and are not appreciably displaced also in the equal mixing case. Surprisingly, the quasi-long-range case in Fig. 14(d) does not differ in any essential way from the other three cases.

Figure 15 illustrates the dependence of the scattering volume on the nonresonant light intensity for three different asymptotic orientations α. The calculations were performed with three channels and for $x_{00} = 0.15$ r.u., i.e., for a field-free s-wave scattering length equal to 1.16 r.u. These values have been chosen in order to present $\ell = 1$ singularities for both m values at an intensity that is not too high; cf. Fig. 2. For $\alpha = 0$, shown in Fig. 15(a), only the $m = 0$ term of the Hamiltonian Eq. (24) contributes, and a singularity is observed at $\mathcal{I} = 1.35$ r.u. with a width of 3.68 r.u. The second singularity in Fig. 15(a) is a consequence of the quasiperiodicity of the model. For $\alpha = \pi/2$, only the $|m| = 1$ term in Eq. (24) comes into play, and the singularity in Fig. 15(b) is found at much higher intensity, $\mathcal{I} = 12.45$ r.u. (with a width of 1.21 r.u.). Whereas the position of the pole in the equal mixing case ($\alpha = \pi/4$), cf. Fig. 15(c), is intermediate between the positions in the two pure-$|m|$ cases, at $\mathcal{I} = 3.64$ r.u., the dependence of the width (equal to 7.08 r.u. in the mixed case) on orientation is less obvious to explain. This is due to the strong dependence of the width on the intensity, which is increasing for $m = 0$ and decreasing for $|m| = 1$ in the pure-$|m|$ cases. All of the singularities shown in Fig. 15 are characterized by $\widetilde{\ell} = 1$. The poles for $\widetilde{\ell} = 3$ would appear for smaller s-wave scattering lengths in the chosen intensity domain or at higher intensity for the chosen s-wave scattering length, and those for $\widetilde{\ell} = 5$ are too narrow to have been resolved in the present calculation.

V. CONCLUSIONS

We have studied nonresonant light control of the p-wave scattering volume characterizing collisions of identical spin-polarized fermions at very low energy. To this end, we have employed an asymptotic model [19,25] to describe the low-energy collisions. This is justified by the predominance of long-range forces at these energies. The short-range interactions are represented by a single parameter, the nodal parameter, in the asymptotic model. It can be fixed if the field-free s-wave scattering length of the collision partners is known [25]. Since the interaction with the nonresonant light scales asymptotically as $1/R^3$ with the interparticle distance, it was necessary to first generalize the definition of the scattering volume; cf. Paper I [29].

For free particles or weak confinement, we have determined when singularities of the field-dressed scattering volume occur as a function of the nonresonant light intensity and of either the field-free s-wave scattering length or the nodal parameter, i.e., the specific colliding pair. The singularities indicate the appearance of a bound state at threshold and correspond to infinitely strong interactions between the identical spin-polarized fermions, thus greatly enhancing the rates of formation of molecules in all-optical association processes of ultracold fermions. As a result, for a given pair of particles, intensities close to a singularity offer the most efficient control over the collisions. The necessary intensities are of the order of 1 GW/cm^2, with the lowest intensities required for strongly polarizable particles with large reduced mass. Such intensities are challenging but feasible with current experimental technology.

Our findings are quite similar to those of our earlier study on using nonresonant light to control the s-wave scattering length for identical bosons or nonpolarized fermions [19]. The main difference is that, at least for certain species, various efficient means to control the s-wave scattering length exist, most notably magnetic field control of Feshbach resonances [6]. In contrast, external field control of the p-wave scattering volume has remained an open goal. This may make the generation of the required nonresonant light intensities a worthwhile experimental endeavor.

We have also considered nonresonant light control of p-wave collisions for strongly confined particles, assuming an isotropic, harmonic 3D trap. In this case, the asymptotic phase shift of the scattering wave function is replaced by an energy shift of the trap states. The energy shift for the odd-ℓ trap states can be directly related to the scattering volume of free collisions. The same is true for s-wave scattering where the even-ℓ trap state energy shift is correspondingly related to the scattering length.

When the intensity of the nonresonant light is varied in a range where we expect the field-dressed scattering volume for free collisions to diverge, the trap states get strongly

perturbed. The perturbation may be so strong as to permit up- or downward climbing of the trap ladder. Under these conditions, it will also be possible to create bound molecular states by slowly varying the nonresonant light intensity. In the vicinity of the divergences, the trap state energy shifts can be directly related to the scattering volume. In contrast, away from the resonance, the trap states keep their character.

Being of essentially $\ell = 1$ character (even in the presence of nonresonant light), p-wave scattering implies a mixing of the states with $m = 0$ and $|m| = 1$. The relative weights of the m states fix the most probable relative orientation of light polarization and interparticle axis. In a single-channel approximation, the orientation for two particles at close range tends to a more or less fixed value. This value generally depends on the asymptotic orientation, except in the proximity of a divergence of the scattering volume. In the latter case, the short-range orientation is such that the particles are approximately head to tail if the pole corresponds to an attractive interaction ($m = 0$). Conversely, if the pole corresponds to a repulsive interaction ($|m| = 1$), the interparticle axis becomes approximately perpendicular to the light polarization. Coupled-channel calculations with three values of ℓ and all corresponding m values have confirmed and amplified these results. While in an experiment the orientation of the dipole moments (induced or permanent) can be imposed by an external field, it is in general nontrivial to fix the orientation of the interparticle axis and thus the weights of the m states which determine the anisotropic deformation of an expanding cloud [61].

In the present calculations, we have used "universal" nodal lines with a single energy-, partial-wave-, and intensity-dependent parameter, the nodal parameter, which in turn only depends on the field-free s-wave scattering length [18]. Our predictions of the nonresonant light intensity required to observe these phenomena could be made more precise by a better account of the short-range interactions, using realistic nodal lines adjusted to experimental data. This modification will be important in particular for collisions at somewhat higher energy, for example when studying shape resonances [18,25,62].

The asymptotic model used here to describe the interaction of polarizable particles with nonresonant light is not restricted to this physical setting. Most importantly, collisions of aligned polar particles at ultralow energies yield the same asymptotic Hamiltonian. It is merely the meaning of the reduced units that changes, and the anisotropic $1/R^3$ interaction is due to the dipole moments of the colliding particles. As a consequence, the calculations presented here also predict the p-wave scattering volume (without any external field) as a function of the dipole moments. Of course, in this case, the effective dipolar interaction strength cannot as easily be tuned as in the case of nonresonant light control.

Given the generality of the asymptotic model with anisotropic $1/R^3$ interaction, a natural extension of the present work would be to explore the dynamics of two interacting ultracold dipoles confined in an only axially symmetric harmonic potential. The investigation of eigenenergies and eigenfunctions is possible for different geometries of the trapping potential, from a pancake-shaped to a cigar-shaped trap, all the way down to quasi-two-dimensional regimes. The trap geometry is known to influence the stability and excitations of dipolar gases [63,64]. In particular, one could design sample shapes that impose a specific orientation, or in other words, fix the weights of the m states. This is intriguing in view of the different character of the p-wave scattering volume singularities for $m = 0$ and $|m| = 1$ states that we have observed here. A further extension would be to consider anharmonic traps.

TABLE III. Parameters A and B of Eq. (13). $\Delta\mathcal{E}_{N,\ell=1,m}$ is the energy shift from the unperturbed energy $\mathcal{E}_0 = 2\beta_\omega^2(2N + 5/2)$ of a trapped $\ell = 1$ state of a pair of particles submitted to a nonresonant light of reduced intensity $\mathcal{I}$ and $\mathcal{M}_0^m(x_{00})$ is the field-dressed scattering volume of the pair when untrapped. The m and $\mathcal{I}$ dependences are those of the c_3 coefficient of the adiabatic $\ell = 1$, m field-dressed potential $c_3 = 4\mathcal{I}/15$ $(-2\mathcal{I}/15)$ for $m = 0$ ($|m| = 1$), cf. Table I in Paper I [29]. All data are in reduced units.

N	$\mathcal{E}_0$	A	B
0	$5\beta_\omega^2$	$-\frac{4\beta_\omega^3 c_3}{3\sqrt{\pi}}$	$\frac{8\beta_\omega^5}{\sqrt{\pi}}$
1	$9\beta_\omega^2$	$-\frac{26\beta_\omega^3 c_3}{15\sqrt{\pi}}$	$\frac{20\beta_\omega^5}{\sqrt{\pi}}$
2	$13\beta_\omega^2$	$-\frac{433\beta_\omega^3 c_3}{210\sqrt{\pi}}$	$\frac{35\beta_\omega^5}{\sqrt{\pi}}$

ACKNOWLEDGMENTS

Laboratoire Aimé Cotton is Unité mixte UMR 9188 du CNRS, de l'Université Paris-Sud, de l'Université Paris-Saclay et de l'ENS Paris-Saclay, member of the Fédération Lumière Matière (LUMAT, FR2764) and of the Institut Francilien de Recherche sur les Atomes Froids (IFRAF). R.G.F. gratefully acknowledges financial support by the Spanish Project No. FIS2014-54497-P (MINECO) and by the Andalusian research group FQM-207. This study has been partially financed by the Consejera de Conocimiento, Investigación y Universidad, Junta de Andalucía and European Regional Development Fund (ERDF), ref. SOMM17/6105/UGR.

APPENDIX A: SCALING PARAMETERS CONNECTING TRAP ENERGY SHIFT AND SCATTERING VOLUME

We present here a general procedure to determine the parameters of the linear transformation Eq. (13) connecting the trap energy shift and field-dressed scattering volume discussed in Sec. III C.

Since A corresponds to a constant shift of the harmonic oscillator levels due to the presence of the interactions, cf. Eq. (13), it is natural to evaluate it by treating the long-range interactions in the atom pair as perturbation of the pure isotropic harmonic oscillator states. To first order, the van der Waals interaction $-1/x^6$ gives rise to a contribution proportional to β_ω^6, whereas the anisotropic term $-c_3/x^3$ results in the dominant contribution to the energy shift. It is proportional to β_ω^3 and negative for $\ell = 1$, $m = 0$ or $\ell \geqslant 3$, $|m| = 0, 1$, when the adiabatic potential is attractive, and positive for $\ell = |m| = 1$, when the potential is repulsive. The expression of the dominant term of A is reported in Table III. An analytical evaluation of the parameter B is obtained by representing the short-range interactions for each partial wave by a contact potential, with strength propor-

tional to the energy-dependent scattering parameter $\mathcal{S}_\ell(E) = [a_\ell(E)]^{2\ell+1}$ for the corresponding ℓ-wave collision [2,3]. In the single-channel approximation, the energy of the trapped bound levels is related to the scattering parameter $\mathcal{S}_\ell(E)$ by an implicit transcendental ℓ-dependent equation involving reduced units of the harmonic oscillator, cf. Eqs. (11) and (12),

$$\mathcal{S}_\ell(E)/(a_\omega)^{2\ell+1} = \underline{f_\ell}(e_\omega), \tag{A1}$$

where $\underline{f_\ell}(e_\omega)$ is expressed analytically in terms of Γfunctions and depends only on the reduced energy e_ω [54,55,57,58]. Equation (A1) implicitly connects the trap state energy of the particles, that interact via an energy-dependent short-range interaction, to the scattering parameter. For scattering in tight traps, it is essential to introduce energy-dependent scattering parameters since the Wigner threshold law may not apply at a given trap energy [58].

Equation (A1) has to be solved self-consistently for each eigenenergy. If we consider, for example, $\mathcal{S}_{\ell=1}(E) = 0$, which corresponds to vanishing short-range interactions in the p wave, Eq. (A1) possesses several roots $E_{N,\ell=1,m}$, each one associated with a state of the unperturbed isotropic 3D harmonic oscillator level $e_\omega = 2N + \ell + 3/2\,\text{r.u.}(\omega)$. A value of the parameter B, which accounts for the short-range interaction to first order in perturbation theory, is analytically obtained from the derivative of the function $\underline{f_\ell}(e_\omega)$ for a vanishing value of the scattering parameter. In van der Waals reduced units, one has

$$B = \left.\frac{dE}{d(\mathcal{S}_{\ell=1}(E))}\right|_{\mathcal{S}_{\ell=1}(E)=0} = 2\beta_\omega^5 \left.\frac{de_\omega}{d(\underline{f_{\ell=1}}(e_\omega))}\right|_{e_\omega=2N+5/2}. \tag{A2}$$

The values obtained for B, which vary as β_ω^5, are reported in Table III. For the lowest trap level, the energy shift is identical to Eq. (15). For $N = 2$ and all other parameters as in Fig. 6 (resp., Fig. 7), the shift A becomes -0.0002327 r.u. (resp., 0.0001163 r.u.), to be compared to -0.00026685 r.u. (resp., 0.000111 r.u.) as quoted in the figure captions. The multiplicative factor $B = 6.17 \times 10^{-6}$ r.u., which is the same for $m = 0$ and $|m| = 1$, has to be compared to the value of 5.9×10^{-6} r.u. in the two figure captions.

APPENDIX B: DEPENDENCE OF THE RELATIVE ORIENTATION AT SHORT RANGE ON THE NODAL PARAMETER x_{00}

The x_{00} dependence of the limit of $\eta(x)$ for $x \to x_{00}$, shown in Fig. 9 in Sec. IV, can be also understood by calculating the slopes $D_m(x_0) = u'_m(x_0)$ of the two solutions $u_{m=0,\pm1}$ at the position of their energy-, intensity-, and ℓ-dependent repulsive wall, $x_0(\mathcal{E} = 0, \ell, \mathcal{I})$ (defined in Appendix C.2 of Paper I [29] and Ref. [18]). This is shown in Fig. 16, where the x_{00} dependence of the ratio $D_0(x_0)/D_1(x_0)$ and that of its inverse are presented. These ratios are independent of α, the asymptotic main orientation. A divergence of the ratio $D_0(x_0)/D_1(x_0)$ appears when the scattering volume diverges for $m = 0$. This is due to the rapid variation of the amplitude of the oscillations of u_0 with x_{00} in the inner region, associated with a divergence of $D_0(x_0)$, the slope of the function $u_0(x)$ at the position x_0 of the repulsive wall, and is a signature of the presence of a bound state at threshold for $m = 0$. The normalized wave function of this bound state has then a very large amplitude in the inner region, as is the case for a shape resonance. This agrees with the results of the Levy-Keller model using free spherical partial p wave at threshold as reference functions, cf. Paper I [29]. In this model, one has $u(x) \propto x^2 - \mathcal{M}(x)/x$. For small x, the $1/x$ contribution prevails and, when x_{00} varies, the short-range amplitude of $u(x)$ and the scattering volume $\mathcal{M}_0$ diverge for the same x_{00} value. Analogously, and for similar reasons, a divergence in x_{00} of the ratio $D_1(x_0)/D_0(x_0)$ appears when the scattering volume $\mathcal{M}_0$ diverges for $|m| = 1$, associated with an $|m| = 1$–bound state at threshold.

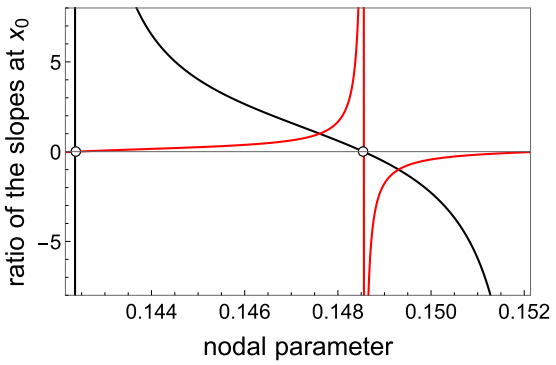

FIG. 16. Dependence on the nodal parameter (in reduced units r.u.) of $D_0(x_0)/D_1(x_0)$, i.e., the ratio of the slopes of the $m = 0$ and the $|m| = 1$ wave functions at the position of their repulsive wall $x_0(\mathcal{E} = 0, \ell = 1, \mathcal{I})$ (in black), together with the x_{00} dependence of the inverse ratio (in red). The intensity is $\mathcal{I} = 6$ r.u. This ratio is independent of the asymptotic main orientation α. The two small open circles indicate the positions of the divergences of the scattering volume for $m = 0$ (left) and $|m| = 1$ (right).

[1] H. Friedrich, *Scattering Theory* (Springer, Berlin, 2016).
[2] A. Derevianko, Phys. Rev. A **67**, 033607 (2003).
[3] Z. Idziaszek and T. Calarco, Phys. Rev. Lett. **96**, 013201 (2006).
[4] P. O. Fedichev, Y. Kagan, G. V. Shlyapnikov, and J. T. M. Walraven, Phys. Rev. Lett. **77**, 2913 (1996).
[5] V. Kokoouline, J. Vala, and R. Kosloff, J. Chem. Phys. **114**, 3046 (2001).
[6] C. Chin, R. Grimm, P. Julienne, and E. Tiesinga, Rev. Mod. Phys. **82**, 1225 (2010).
[7] J. Zhang, E. G. M. van Kempen, T. Bourdel, L. Khaykovich, J. Cubizolles, F. Chevy, M. Teichmann, L. Tarruell, S. J. J. M. F. Kokkelmans, and C. Salomon, Phys. Rev. A **70**, 030702 (2004).
[8] C. H. Schunck, M. W. Zwierlein, C. A. Stan, S. M. F. Raupach, W. Ketterle, A. Simoni, E. Tiesinga, C. J. Williams, and P. S. Julienne, Phys. Rev. A **71**, 045601 (2005).

[9] K. Günter, T. Stöferle, H. Moritz, M. Köhl, and T. Esslinger, Phys. Rev. Lett. **95**, 230401 (2005).

[10] J. P. Gaebler, J. T. Stewart, J. L. Bohn, and D. S. Jin, Phys. Rev. Lett. **98**, 200403 (2007).

[11] Y. Inada, M. Horikoshi, S. Nakajima, M. Kuwata-Gonokami, M. Ueda, and T. Mukaiyama, Phys. Rev. Lett. **101**, 100401 (2008).

[12] M. Waseem, T. Saito, J. Yoshida, and T. Mukaiyama, Phys. Rev. A **96**, 062704 (2017).

[13] S. Blatt, T. L. Nicholson, B. J. Bloom, J. R. Williams, J. W. Thomsen, P. S. Julienne, and J. Ye, Phys. Rev. Lett. **107**, 073202 (2011).

[14] R. Yamazaki, S. Taie, S. Sugawa, K. Enomoto, and Y. Takahashi, Phys. Rev. A **87**, 010704 (2013).

[15] M. Yan, B. J. DeSalvo, B. Ramachandhran, H. Pu, and T. C. Killian, Phys. Rev. Lett. **110**, 123201 (2013).

[16] R. González-Férez and C. P. Koch, Phys. Rev. A **86**, 063420 (2012).

[17] M. Tomza, R. González-Férez, C. P. Koch, and R. Moszynski, Phys. Rev. Lett. **112**, 113201 (2014).

[18] A. Crubellier, R. González-Férez, C. P. Koch, and E. Luc-Koenig, New J. Phys. **17**, 045020 (2015).

[19] A. Crubellier, R. González-Férez, C. P. Koch, and E. Luc-Koenig, Phys. Rev. A **95**, 023405 (2017).

[20] B. Gao, Phys. Rev. A **58**, 4222 (1998).

[21] B. Gao, Phys. Rev. A **64**, 010701 (2001).

[22] B. Gao, J. Phys. B **36**, 2111 (2003).

[23] A. Crubellier and E. Luc-Koenig, J. Phys. B **39**, 1417 (2006).

[24] B. Gao, Phys. Rev. A **80**, 012702 (2009).

[25] B. E. Londoño, J. E. Mahecha, E. Luc-Koenig, and A. Crubellier, Phys. Rev. A **82**, 012510 (2010).

[26] M. Marinescu and L. You, Phys. Rev. Lett. **81**, 4596 (1998).

[27] V. Roudnev and M. Cavagnero, J. Phys. B **42**, 044017 (2009).

[28] J.-L. Bohn, M. Cavagnero, and C. Ticknor, New J. Phys. **11**, 055039 (2009).

[29] A. Crubellier, R. González-Férez, C. P. Koch, and E. Luc-Koenig, preceding paper, Phys. Rev. A **99**, 032709 (2019).

[30] P. Schwerdtfeger, in *Computational Aspects of Electric Polarizability Calculations: Atoms, Molecules, and Clusters*, edited by G. Maroulis (IOS Press, Amsterdam, 2006), pp. 1–32.

[31] P. G. Mickelson, Y. N. Martinez de Escobar, M. Yan, B. J. De Salvo, and T. C. Killian, Phys. Rev. A **81**, 051601(R) (2010).

[32] S. Stellmer, R. Grimm, and F. Schreck, Phys. Rev. A **87**, 013611 (2013).

[33] T. Fukuhara, Y. Takasu, M. Kumakura, and Y. Takahashi, Phys. Rev. Lett. **98**, 030401 (2007).

[34] M. Kitagawa, K. Enomoto, K. Kasa, Y. Takahashi, R. Ciurylo, P. Naidon, and P. S. Julienne, Phys. Rev. A **77**, 012719 (2008).

[35] G. Cappellini, M. Mancini, G. Pagano, P. Lombardi, L. Livi, M. Siciliani de Cumis, P. Cancio, M. Pizzocaro, D. Calonico, F. Levi *et al.*, Phys. Rev. Lett. **113**, 120402 (2014).

[36] K. K. Ni, S. Ospelkaus, M. de Miranda, A. Pe'er, B. Neyehuis, J. J. Zirbel, S. Kotochigova, P. S. Julienne, D. S. Jin, and J. Ye, Science **322**, 231 (2008).

[37] S. Ospelkaus, K.-K. Ni, G. Quéméner, B. Neyenhuis, D. Wang, M. H. G. de Miranda, J. L. Bohn, J. Ye, and D. S. Jin, Phys. Rev. Lett. **104**, 030402 (2010).

[38] J. Deiglmayr, A. Grochola, M. Repp, O. Dulieu, R. Wester, and M. Weidemüller, Phys. Rev. A **82**, 032503 (2010).

[39] T. Shimakasi, J. T. Kim, and D. DeMille, ChemPhysChem **17**, 3677 (2016).

[40] K. K. Ni, S. Ospelkaus, D. Wang, G. Quéméner, B. Neyenhuis, M. H. G. de Miranda, J. L. Bohn, J. Ye, and D. S. Jin, Nature (London) **464**, 1324 (2010).

[41] M. H. G. de Miranda, A. Chotia, B. Neyenhuis, D. Wang, G. Quéméner, S. Ospelkaus, J. L. Bohn, J. Ye, and D. Jin, Nat. Phys. **7**, 502 (2011).

[42] M. Lepers, R. Vexiau, M. Aymar, N. Bouloufa-Maafa, and O. Dulieu, Phys. Rev. A **88**, 032709 (2013).

[43] B. Pasquiou, G. Bismut, Q. Beaufils, A. Crubellier, E. Maréchal, P. Pedri, L. Vernac, O. Gorceix, and B. Laburthe-Tolra, Phys. Rev. A **81**, 042716 (2010).

[44] B. Taylor, A. Reigue, E. Maréchal, O. Gorceix, B. Laburthe-Tolra, and L. Vernac, Phys. Rev. A **91**, 011603(R) (2015).

[45] M. Lu, N. Q. Burdick, and B. L. Lev, Phys. Rev. Lett. **108**, 215301 (2012).

[46] Y. Tang, A. Sykes, N. Q. Burdick, J. L. Bohn, and B. L. Lev, Phys. Rev. A **92**, 022703 (2015).

[47] K. Aikawa, A. Frisch, M. Mark, S. Baier, R. Grimm, and F. Ferlaino, Phys. Rev. Lett. **112**, 010404 (2014).

[48] A. Frisch, M. Mark, K. Aikawa, S. Baier, R. Grimm, A. Petrov, S. Kotochigova, G. Quéméner, M. Lepers, O. Dulieu, and F. Ferlaino, Phys. Rev. Lett. **115**, 203201 (2015).

[49] M. Lepers, J.-F. Wyart, and O. Dulieu, Phys. Rev. A **89**, 022505 (2014).

[50] S. Kotochigova and A. Petrov, Phys. Chem. Chem. Phys. **13**, 19165 (2011).

[51] For instance, choice of the nodal parameters fixes the *s*-wave scattering length (in the absence of nonresonant light).

[52] The values of the scattering lengths are taken from Table I of Ref. [25].

[53] B. Gao, Eur. Phys. J. D **31**, 283 (2004).

[54] K. Kanjilal, J. L. Bohn, and D. Blume, Phys. Rev. A **75**, 052705 (2007).

[55] K. Kanjilal and D. Blume, Phys. Rev. A **70**, 042709 (2004).

[56] T. Stöferle, H. Moritz, K. Günter, M. Köhl, and D. Esslinger, Phys. Rev. Lett. **96**, 030401 (2006).

[57] T. Busch, B.-G. Englert, K. Rzazewski, and M. Wilkens, Found. Phys. **28**, 549 (1998).

[58] E. Bolda, E. Tiesinga, and P. Julienne, Phys. Rev. A **66**, 013403 (2002).

[59] D. Bortolotti, S. Ronen, J. Bohn, and D. Blume, Phys. Rev. Lett. **97**, 160402 (2006).

[60] S. Ronen, D. Bortolotti, J. Bohn, and D. Blume, Phys. Rev. A **74**, 033611 (2006).

[61] J. Stuhler, A. Griesmaier, T. Koch, M. Fattori, T. Pfau, S. Giovanazzi, P. Pedri, and L. Santos, Phys. Rev. Lett. **95**, 150406 (2005).

[62] A. Crubellier, R. González-Férez, C. P. Koch, and E. Luc-Koenig, New J. Phys. **17**, 045022 (2015).

[63] S. Yi and L. You, Phys. Rev. A **61**, 041604(R) (2000).

[64] S. Yi and L. You, Phys. Rev. A **66**, 013607 (2002).